Physical properties of high-pressure plasmas

V. A. Alekseev, V. E. Fortov, and I. T. Yakubov

I. V. Kurchatov Institute of Atomic Energy, Moscow; Institute of Chemical Physics, Academy of Sciences of the USSR; Institute of High Temperatures, Academy of Sciences of the USSR
Usp. Fiz. Nauk **139**, 193–222 (February 1983)

PACS numbers: 52.25. – b

CONTENTS

1. INTRODUCTION

Over the past decade there has been a sharp increase in the interest in high-pressure plasmas, by which we mean plasmas compressed to the extent that interparticle interactions become important. Nonideal plasmas figure in plans for pulsed fusion[1] and fission[2] power reactors, high-power MHD generators,[3] thermoelectric energy convertors,[4] and other new technological applications. A plasma is nonideal when there is a high concentration of energy in it, e.g., during the passage of strong shock waves,[5] when targets are bombarded by various beams (laser, electron, ion, and neutron beams)[6,7], in high-power pulsed electric discharges, and in other situations. Pressures of tens to hundreds of millions of atmospheres are presently being achieved in the laboratory. Data on the thermodynamic and transport properties of dense plasmas over broad ranges of "nonideality" and degeneracy parameters are urgently needed for predicting the consequences of local energy concentrations of this magnitude.

The properties of high-pressure plasmas have attracted the interest of physicists from some very different fields over the years.[5-14] The question involved here is the behavior of matter over a range of parameters which is quite broad and which also poses extreme difficulties for both theoreticians and experimentalists: the range stretching from dense vapors and liquids up to exotically high densities, pressures, and temperatures, including the hightemperature boiling curves, metal–insulator transition regions, and regions in which hypothetical plasma phase transitions are expected. Active experimental and theoretical research has recently led to the replacement of a large number of heuristic ideas by a more definite understanding of the physics of dense plasmas and has laid the foundation for the construction of corresponding models.

The anomalous properties of a nonideal plasma which have been observed experimentally stem from extremely radical changes in the collective state of the plasma particles: the appearance of heavy electron and ion clusters and collisional complexes, the compression of atoms and ions, and the resulting radical change in the structure of the discrete spectrum. We are now at a point where we can summarize this research; we will also point out directions for future research.

2. THERMODYNAMIC PROPERTIES

Nonideal plasmas span an extremely broad region on a phase diagram (Fig. 1). At low densities, the region is bounded by the condition that the interaction energy becomes equal to the kinetic energy, which is determined by the temperature, $\beta = T^{-1}$:

$$\gamma = e^2 n_e^{1/3} \beta = 1,$$
$$\Gamma = e^2 r_D^{-1} \beta = \sqrt{8\pi}\gamma^{3/2} = 1,$$
$$\gamma_{ae} = \frac{2\pi\alpha e^2 n \beta}{R} = 1.$$

The nonideality parameters γ and Γ are measures of the interaction between charges, n_e is the electron density, and r_D is the Debye length. The parameter γ_{ae} describes the interaction of charged particles with neutrals, α is the atomic polarizability, n is the density of atoms, and R is a scale atomic radius. On the high-density side the nonideality region is bounded for degenerate electrons by the condition $\gamma = e^2 n_e^{1/3} \varepsilon_F^{-1}$, where $\varepsilon_F = \hbar^2 n_e^{2/3}/2m_e$ is the Fermi energy. In a weakly ionized plasma (low values of T) the charge–neutral interaction is important,

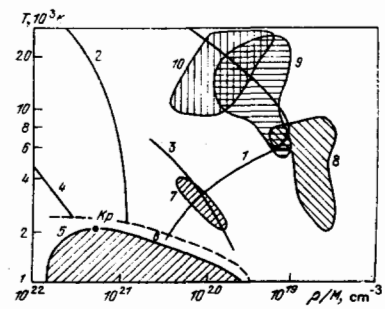

FIG. 1. Phase diagram of cesium. 1—$\Gamma = 1$; 2—$\gamma = 1$; 3—$\gamma_{ea} = 1$; 4—$n_e \lambda_e^3 = 1$; 5, 6—region of static experiments[11,14,15]; 7—adiabatic compression[16,17,22]; 8, 9—compression by incident and reflected shock waves[18,19]; 10—isobaric ohmic heating.[20,21]

 0038-5670/83/020099-17$01.80

while in the highly ionized region the Coulomb interaction is important. Near the boiling point of metals, $\rho \gtrsim \rho_c$, interactions between neutral particles are superimposed on the plasma interactions.

Experiments on nonideal plasmas require high local concentrations of energy in dense media. The pressures and temperatures involved are significantly higher than can be withstood by structural materials, and the conventional methods of plasma diagnostics cannot be used. Only very recently has it become possible to overcome these difficulties. Figure 1 shows the regions in which experiments have been carried out on the thermodynamic properties of a cesium plasma.

Because of the low ionization potential of cesium (3.89 eV), the nonideal cesium plasma is the one which has been studied in most detail, by both static and dynamic methods. Static experiments[11,14,15] have yielded p-V-T data at $T \lesssim 2500$ K, the phase coexistence curves, and the parameters of the critical point. Furthermore, the heat capacities C_p and C_v have been measured[15] in the liquid phase at $T \lesssim 2000$ K over the density range 1.4 g/cm^3 $> \rho >$ 0.8 g/cm^3, approaching the critical density of cesium, ρ_c = 0.4 g/cm^3. In the region of parameters accessible to the static methods the interaction of charges with neutrals is important.

In order to produce plasmas with a high degree of ionization and a strong Coulomb interaction, temperatures even further above the critical temperature are required. The methods being used to reach these temperatures are shock[18,19] and adiabatic[16,17] compression and isobaric ohmic heating in glass capillaries[21] and in inert-gas atmospheres.[20] Pulsed methods[18,19] have made it possible to move a good distance up the temperature scale, to $T = 3 \cdot 10^4$ K, and thereby to produce a doubly ionized plasma with a Coulomb nonideality parameter $\Gamma \approx 3$.

An extremely important question in the thermodynamics of a nonideal plasma is its phase stability. The literature contains many suggestions of exotic phase transitions driven by a strong Coulomb interaction in degenerate systems[23-25] and Boltzmann systems,[26,27] in weakly ionized plasmas upon the metallization of dense metal vapor,[29] and, again in weakly ionized plasmas, as a result of cluster formation.[28] The relationship between the anomalies in the dielectric permittivity of a nonideal plasma and its stability (the excitation of spin- and charge-density waves and the formation of ordinary and coherent crystals) has been analyzed in some comprehensive reviews.[30,31]

Analysis of the p-V-T data presently available on cesium[11,18,19] and mercury[32] and, in particular, experimental results on the specific heat[15] definitely shows that there are no phase anomalies distinguishable from boiling.

In addition, the highest-temperature part of the region of the vapor–liquid phase transition is determined to a significant extent by the strong plasma interaction, since cesium and mercury plasmas are nonideal according to Refs. 12 and 28 near the critical point: γ, $\gamma_{ae} \gtrsim 1$. This conclusion is apparently general in nature, applicable to all metals,[33] since the high binding energies cause the critical temperatures of metals to be extremely high, comparable to the corresponding ionization potentials, which are in turn lowered by the strong interaction in a dense plasma. Consequently, the high-temperature boiling of a metal corresponds to a transition directly to a dense plasma phase, skipping the neutral-vapor region (in contrast with ordinary liquid insulators).

The conclusion that there are no exotic phase anomalies in the liquid-metal state region is also supported by measurements of the unloading isentropes of shock-compressed metals[34] and by data from isobaric ohmic heating[35] (Fig. 2). Particularly indicative are detailed measurements of the static structure factor $S(Q)$ of liquid rubidium,[36] carried out by neutron diffraction (Fig. 3). We see that as the metal is heated and expands the short-range order is lost, and there is a continuous transition to a disordered gaseous state. Curiously, these structural properties of expanding rubidium can be described satisfactorily by the hard-sphere model,[37] which is quite popular in the theory of simple liquids, and which yields a single-phase equation of state at moderate densities.

The data on the equation of state obtained above the critical temperature[18-20] also point to a single-phase composition for a nonideal plasma and provide data for a quantitative test of thermodynamic plasma models (Fig. 4). It turns out[18,19] that the pressure of a cesium plasma does not fall off with increasing Γ, as it should in a Debye plasma; on the contrary, the pressure exceeds that calculated in the ideal-gas approximation (for a mixture of ideal gases: electrons, atoms, and ions). Direct comparison with experiment shows that the ring approximation in a grand canonical ensemble gives a fair description of the situation. This approximation predicts a stable equation of state over the entire range of the nonideality parameter Γ (Ref. 39):

$$\beta p = \sum_k n_k - \sum_j n_j \left(\frac{\Gamma}{6}\right)\left[1 + \frac{\Gamma\varphi(\Gamma)}{2}\right]^{-1}; \qquad (1)$$

here $\varphi(\Gamma)$ is the solution of the equation $\varphi^3 + (2/\Gamma)\varphi^2 - (2/\Gamma) = 0$, the index "$k$" runs over all the plasma components, while the index "j" runs over only the charged components.

This use of (1) goes far beyond the range of applicability of this expression and simply emphasizes the urgent need for a systematic theoretical derivation of the ther-

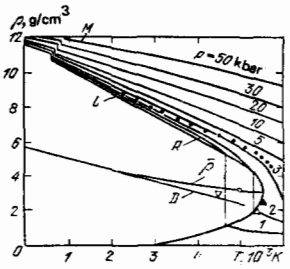

FIG. 2. Boiling curve of copper.[34] Circles—Data from electrical-explosion measurements[35]; curves—calculations from the wide-range equation of state from Ref. 34.

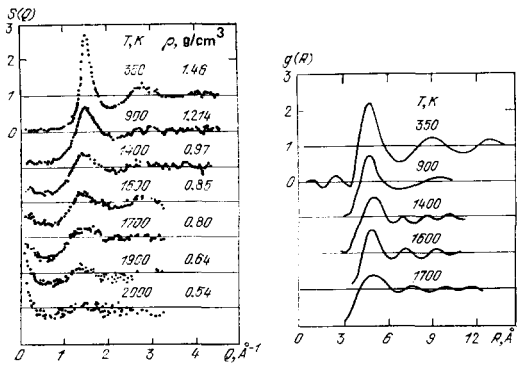

FIG. 3. The static structure factor $S(q)$ and the binary distribution function $g(r)$ of liquid rubidium at various temperatures T and densities ρ.[36]

modynamic functions. This expression is based on an expansion of the Coulomb part of the thermodynamic potential Ω in powers of the electron activity ξ. The difficulties in carrying out this expansion are well known.[8,9] The first few terms are

$$-\frac{\beta\Delta\Omega_{\text{Coul}}}{V}=A\xi^{3/2}+B\xi^{2}\ln\xi+C\xi^{2}+E\xi^{5/2}+D\xi^{5/2}\ln\xi+\ldots. \qquad (2)$$

The first three terms of the series correspond to approximation (1). In (2) we have added the terms $D\xi^{5/2}\ln\xi$ and $E\xi^{5/2}$, which are also generated by polarization effects. The research by Ebeling, Kraeft, and Kremp (see Ref. 8, for example) has played a major role in the derivation of the thermodynamics of plasmas in a grand canonical ensemble. They calculated the coefficients of series (2) in various plasma parameter regions. For cool plasmas ($\chi_e^2/r_D^2 \ll 1$, $\Gamma \ll 1$), the coefficients D and E were found in Ref. 40, where it was pointed out that the contributions of the discrete and continuous spectra to the thermodynamic potential cancel out in a slightly nonideal plasma. We can thus see why the Debye approximation in a grand ensemble is successful.

The use of a diagram technique based on a regrouping and selective summation of the perturbation-theory series has been limited by the small number of expansion parameters and by the conditions for the convergence of these series. Comparison of theory and experiment shows that it is apparently possible to extrapolate these

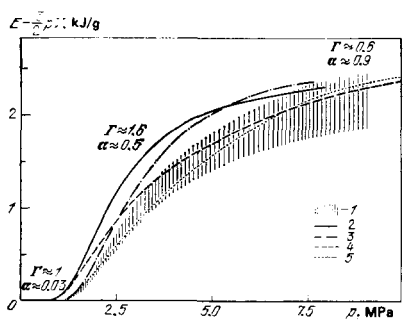

FIG. 4. Enthalpy of a cesium plasma at $V=10^3$ cm^3/g. 1—Experiment; 2—Debye ring approximation in a grand canonical ensemble[39]; 3—model of a "bounded" atom[41]; 4—allowance made for "local electrical neutrality"[42]; 5—model of a bounded atom with local electrical neutrality.[42]

results to $\Gamma = 1$. Several "pseudopotential" models have been advanced to describe plasmas at high values of Γ. In these approaches, the major hypothesis is embodied in the choice of a particular binary potential for the electron–ion interaction. This potential must, first and foremost, describe the quantum-mechanical effects which arise in short-range interactions.[8,13] These models are essentially semiempirical models, since one of the parameters is chosen to fit the experimental data.

It follows from general considerations that the electron-ion pseudopotential must be finite at short distances, while remaining a Coulomb potential at large distances. One such pseudopotential is

$$\Phi_{ie}=-\frac{z_i e^2}{r}[1-\exp(-r\varkappa)]. \qquad (3)$$

This one was used in Refs. 41 and 42, where the binary correlation function was written in the form

$$F(r)=1\pm\frac{A(e^{-qr}-e^{pr})}{r}=1\pm\psi_0 e^{-\nu r}\frac{\operatorname{sh}\omega r}{\omega r}. \qquad (4)$$

An expression with the general form (4) is found for potential (3) in the ring approximation at $\Gamma \ll 1$. The free parameters A, p, and q (or ψ_0, ν, and ω) are determined by the charge and dipole-moment screening conditions[42] and also by the relationship between the amplitude of the screening cloud, ψ_0, and the depth of the pseudopotential, $\Phi_{ei}(0)$:

$$n\int(F_+-F_-)\,dr=1, \qquad (5)$$

$$n\int(F_+-F_-)\frac{r^2}{r_D^2}\,dr=3, \qquad (6)$$

$$-\psi_0\approx\ln F_+\approx(\Phi_{ei}-\Delta\mu_e-\Delta\mu_i)\,T^{-1}. \qquad (7)$$

Corrections to the thermodynamic functions for (3) and (4) are then calculated by the standard method[41] and contain the sole semiempirical parameter of the model: the pseudopotential depth $\Phi_{ei}(0)$. Comparison with experimental results on cesium shows that the depth of pseudopotential (3) is

$$\Phi_{ei}(0)=T, \qquad (8)$$

i.e., approximately equal to the energy which distinguishes free electrons from bound electrons. It is important to note that this choice is quite universal, since it can also explain experiments on the shock compression of highly nonideal argon and xenon plasmas.[41,43]

The Monte Carlo pseudopotential model[13] is based on a computer calculation of the average thermodynamic quantities for a given interparticle potential. Exhaustive computer calculations have been carried out for a system of point charged particles against a background of a uniformly distributed neutralizing charge of the opposite sign, and a detailed study has been made of the thermodynamic structural and transport properties over the entire range of nonideality parameters (see Refs. 27, 25, 44, 45, and the literature cited there).

In a real, multicomponent plasma, quantum-mechanical effects are of fundamental importance, stabilizing the Coulomb system and giving rise to bound states.

Binary quantum effects were taken into account most comprehensively by Zelener *et al.*[13] The pseudopotential of the electron–ion interaction was determined by setting the quantum-mechanical probability density equal to the classical correlation function (the contribution of the discrete spectrum was singled out). Since this procedure requires using electron wave functions (not known at the outset for a nonideal plasma), the specific calculations were carried out with a model pseudopotential of the type

$$\Phi_{ei}(r, T) = -\frac{e^2}{r}, \quad r > \sigma; \quad \Phi_{ei}(T) = -\varepsilon T \quad r \leqslant \sigma, \quad \sigma = \frac{e^2}{\varepsilon T}. \qquad (9)$$

The numerical parameter $\varepsilon \approx 2$ was chosen on the basis of experimental data. The well depth $\Phi_{ei}(0, T)$ turned out to be significantly greater than in model (3), (4).

The applicability of pseudopotential models is limited by the need to know the energy spectrum of the bound states. In a dense plasma the discrete spectrum is not known at the outset and may be greatly distorted by the strong interaction. Conditions of this type have been arranged in the explosive compression of argon and xenon[41,43,46,47] (Fig. 5). Extremely high temperatures (up to $8 \cdot 10^4$ K) and pressures (up to 100 kbar) have been achieved; the corresponding densities, $\rho \approx 2$–3 g/cm^3, are above the critical value. Under these conditions the strong interparticle interactions affect not only the free electrons ($\Gamma \approx 5$) but also the bound states of electrons in ions and atoms. The average interparticle distance in a compressed plasma is comparable to the scale dimension of heavy particles. Incorporating the interparticle repulsion in the virial equation[52] has improved the agreement of the pseudopotential model with experiment. This approach, however, made it clear that the states of the discrete spectrum must be taken into account correctly. This was done in Ref. 41 in the model of a "bounded" atom, which describes the effect of the medium on the bound electrons through an effective potential:

$$\Phi_{ei}(r) = -z_i \frac{e^2}{r}, \quad r < r_c; \quad \Phi_{ei}(r) = \infty, \quad r \geqslant r_c. \qquad (10)$$

To find the eigenfunctions and excitation energies, a version of the Hartree-Fock method is used, based on a numerical solution of the Schrödinger equations for the radial part of the electron wave function. This solution determines the energy spectrum of the compressed atom as a function of the degree of compression, of which the parameter r_c is a measure. The results of these calculations were subsequently used to determine the thermodynamic properties of plasmas. The equilibrium value of r_c corresponding to given values of V and T is determined by the variational principle

$$\left(\frac{\partial F}{\partial r_c}\right)_{V,T} = 0. \qquad (11)$$

The expression for the free energy F includes corrections for the Coulomb interaction of the free charges and the interparticle repulsion in the hard-sphere approximation,[48,37]

$$\Delta F_s = NT(3y-4)(y-1)^{-2}y, \quad y = (4\pi/3)Nr_c^3. \qquad (12)$$

The model of a bounded atom gives a satisfactory description of the increase in the pressure of a nonideal plasma which is observed experimentally (Fig. 5). We might note that those models which ignore the distortion of the discrete spectrum indicate a decrease in the plasma pressure because of its polarization compression. In Section 4 of this review we will use the model of a bounded atom to interpret optical measurements.

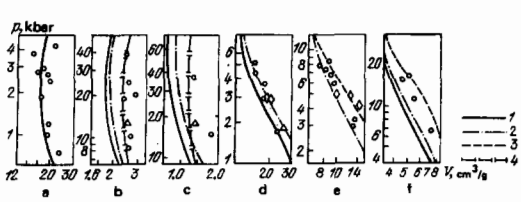

FIG. 5. Shock adiabatics of nonideal plasmas. Xenon: a—p_0 = 1 bar; b—10; c—20. Argon: d—p_0 = 1 bar; e—5; f—20. 1—Debye ring approximation[39]; 2—additional incorporation of atomic repulsion in the second virial coefficient[52]; 3—model of a "bounded atom," (10), (11) (Ref. 41); 4—pseudopotential model, (3)–(7) (Ref. 41).

Researchers have moved to higher densities and pressures (pressures of the order of a megabar) by using some methods new to plasma physics. Thermodynamic properties were studied in Refs. 34, 49, and 50 by observing the adiabatic expansion of metal samples compressed beforehand by intense shock waves. Measurements of this type provide a unique opportunity for studying the behavior of matter from the condensed state (pressures of the order of a megabar), where the ions are highly disordered, while the electrons are degenerate, up to a nearly ideal Boltzmann plasma, including curves of high-temperature melting and boiling. The experiments of Refs. 34, 49, and 50 span four orders of magnitude in pressure and two in density. As a dense plasma expands, a variety of obscure physical processes occur in it: The electron degeneracy is lifted; the electron energy spectrum is changed; the plasma recombines; the ion component becomes disordered: a "metal–insulator" phase transition occurs; and a highly nonideal gaseous plasma forms. These experiments have made it possible to extract thermodynamic information in a region of the phase diagram which had not previously been studied and which poses extreme difficulties theoretically. In particular, it has been shown that no "plasma" phase transitions occur in the region studied.

The experimental data have been used to construct semiempirical equations of state for nonideal plasmas.[34] In these models, the entire set of static and dynamic data in the solid, liquid, and gas phases is described in a common analytic form; melting, evaporation, thermal ionization, ionization by pressure, and the lifting of the electron degeneracy are all reproduced. The semiempirical equation of state has the correct Debye-Hückel and Thomas-Fermi asymptotic expressions. It is convenient for hydrodynamic calculations for physical events which result from a pulsed local concentration of energy in a plasma.[51]

3. ELECTRICAL CONDUCTIVITY AND THERMOELECTROMOTIVE FORCE OF A WEAKLY IONIZED PLASMA

The electron transport coefficients of a plasma are more sensitive to nonideality effects than are the ther-

modynamic properties. Furthermore, electrophysical measurement methods are more sophisticated. These circumstances apparently explain why a rather large amount of corresponding experimental information is already available. Significantly, the results obtained in recent years in the various laboratories are in fair agreement with each other. It should be kept in mind that the results have been obtained at high temperatures, where the problem of structural materials, especially electrical insulating materials, is an acute one.

A general picture of the electrical conductivity of metals can now be drawn over the entire range of parameters. Figure 6 shows the static electrical conductivity σ of cesium. The corresponding experiments were carried out during steady-state heating of measurement cells in furnaces[53-55] and during Joule heating[21] in adiabatic[17,22] and shock[56] tubes.

At low values of T the values of σ measured at extreme pressures differ by many orders of magnitude (in the cases of the weakly ionized gas and the metal). At high T the plasma is approaching an ideal plasma, and all the isobars should approach the values of σ of a highly ionized plasma, given by the Spitzer expression $\sigma \sim T^{3/2} \ln\Lambda$, where $\ln\Lambda$ is the Coulomb logarithm. Since $\ln\Lambda$ depends only slightly on the pressure at high T, the values of σ are of the same order of magnitude on all the isobars in Fig. 6.

At low pressures, $p \ll p_c$, the conductivity increases monotonically with increasing T, since the degree of thermal ionization of the plasma is increasing. At $p \gtrsim p_c$ the conductivity, beginning with values typical of liquid metals, falls off sharply upon heating: A metal-insulator transition occurs. The transition from the metallic state to the plasma state has many common features in different materials (Fig. 7). Despite the different conductivity level of metals, the sharpest decrease in σ on the supercritical isobars ($p \lesssim 2p_c$) occurs from the value 200 mho/cm, typical of $T \approx T_c$.

In Fig. 6 the isobar p = 1 bar draws an arbitrary boundary between the ideal and nonideal plasmas of cesium vapor. At $p \gtrsim 1$ bar the plasma conductivity increases with increasing pressure,

$$d\sigma/dp > 0, \tag{13}$$

while at $p \lesssim 1$ bar we find

$$d\sigma/dp < 0, \tag{14}$$

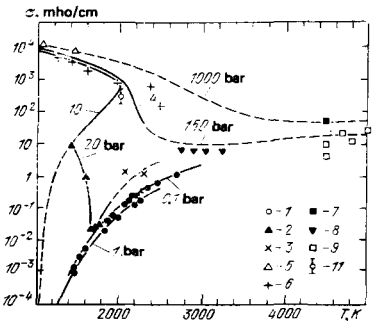

FIG. 6. σ isobars of cesium according to the data of Refs. 53 (1), 54 (2), 55 (3–5), 21 (6, 7), 17 (8), and 56 (9). On the phase-equilibrium line: Ref. 55 (10) and Ref. 36 (11).

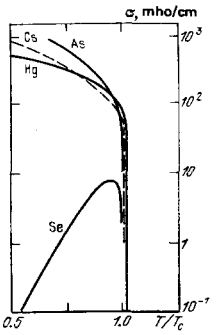

FIG. 7. σ isobars in the metal-insulator transition region ($p = 2p_c$; Ref. 38).

as in an ideal plasma. The behavior of the conductivity of a nonideal plasma is the most interesting. With decreasing T the conductivity goes through a minimum at $T = T_{min}$ and increases at $T < T_{min}$.

Significantly, the conductivity of cesium vapor reaches anomalously high values on the saturation line—values five or six orders of magnitude higher than the results of ordinary ideal-gas estimates. The high values of the conductivity of a nonideal plasma, combined with the retention of a compressibility similar to that of a gas, make nonideal plasmas promising as the working medium for MHD generators.[3]

The observed anomalies in the conductivity of a weakly ionized plasma stem from the interaction of charges with neutrals, which are manifested in the formation of charged clusters and in the deformation of the atomic energy terms. Even in a slightly nonideal plasma the ion-atom interaction gives rise to an A_2^+ ion and a lowering of the ionization potential, ΔI_i. It is a simple matter to derive,[12] in place of the ordinary Saha equation, the following:

$$n_e^+ \approx n\lambda_e^{-3} \exp[-(I - \Delta I_i)\beta] \cdot [1 + nk_2 \exp(D_2^+\beta)]. \tag{15}$$

Here I is the ionization potential of the atom, $k_2(T)$ is the constant of the dissociative equilibrium $A_2^+ \rightleftharpoons A^+ + A^+$, and D_2^+ is the binding energy of A_2^+. Nonideality increases n_e. Expression (15) incorporates the ion-atom interaction in the continuous and discrete spectra (ΔI_i and A_2^+). Furthermore, the electron–atom interaction gives rise to an A^- ion and lowers the ionization potential, ΔI_e, under the same conditions. In Fig. 8, the regions of strong and weak ion–atom and electron-atom interactions are separated in the continuous and discrete spectra. The characteristics of various alkali complexes are given in Ref. 57.

At high values of T (Fig. 8) the primary effect in a dense plasma is a lowering of the ionization potential. Assuming $\sigma \sim n_e$, i.e., that the mobility varies only slightly, we can write[58,59]

$$\sigma = \sigma_0 \exp\left[-(I - \Delta I)\frac{\beta}{2}\right], \quad \Delta I = \Delta I_i + \Delta I_e; \tag{16}$$

here σ_0 is a constant, ΔI is the lowering of the ionization potential caused by the interactions of ions and electrons with atoms, $\Delta I_i = 1.61 \cdot 4\pi Tn(\alpha e^2\beta/2)^{3/4}$ (Ref. 39), $\Delta I_e = -2\pi\hbar^2 Ln/m$ (the optical approximation), and

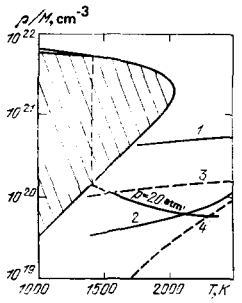

FIG. 8. Density-temperature diagram of cesium.[12] 4—$\Delta I_e = T$; 3—$\Delta I_i = T$; 2—$n^- = n_e$; 1—$n_2^+ = n^+$; 5—the isobar $p = 2$ bar.

L is the scattering length for the scattering of an electron by an atom. Since $\Delta I \sim n$, the conductivity increases exponentially with increasing n at $n > n^*$. Estimates[58] yield $n^* \approx 10^{20}$ cm^{-3} in cesium, in agreement with experiment.

At low temperatures nonideality occurs because charged particles form clusters.[28,12] Even in a slightly nonideal plasma the predominant ion species becomes heavier as T decreases along the isobar $p = 20$ bar. At $T < 1650$ K we have $n^+ < n_2^+ < n_3^+$; i.e., Cs_3^+ becomes the predominant ion species.[60] As T is lowered, Cs_m^+ ions with $m \gg 1$ appear. In an alkali plasma the number of negatively charged clusters Cs_m^- is comparatively low. Their binding energies are significantly lower than those of positively charged clusters (Fig. 9), so that the difference $(n_m^+ - n_m^-)$ increases toward the saturation line, and the electron density therefore increases[1]: $n_e = n_m^+ - n_m^-$.

The effect of clusters on the conductivity of a dense plasma was first taken up by Khrapak and Yakubov.[65] A cluster is a bound state of a charged particle with the surrounding medium. A classical approach can be taken to describe an ion cluster. The attractive forces acting between an ion and atoms (primarily polarization forces) cause the atoms to accumulate near the ion, and the ion becomes trapped in the resulting potential well. The number of particles in an ion cluster is approximately the same as the number of excess atoms around the ion. If for simplicity we ignore the atom–atom and electron–atom interactions, we can write the number of particles in a cluster as $m = n \int dr [\exp(-\beta V_i(r)) - 1]$, where $V_i(r)$ is the ion–atom interaction energy (see Refs. 12 and 64 for the more detailed expressions). The free energy of the plasma decreases, $\Delta F_i = -Tmn^+$, leading to the following equation for an ionizational equilibrium:

$$n_e^+ = n\lambda_e^{-3} \exp(-\beta I + m). \tag{17}$$

Assuming $\sigma \sim n_e$, we find

$$\sigma \approx \sigma_0 \exp\left[-\tfrac{1}{2}\beta I + \tfrac{1}{2} n v_0 \exp(g\beta)\right], \tag{18}$$

where g and v_0 are the depth and effective volume of the potential $V_i(r)$. The quantity g seems to be approximately equal to D_2^+, the dissociation energy of the A_2^+ ion. Expression (18) gives a qualitatively correct description of the behavior of $\sigma(P, T)$ in Fig. 6. The isobar $\sigma(T)$ has a minimum at

$$T_{\min} \approx \frac{g}{\ln(I/gnv_0)}. \tag{19}$$

At $T < T_{\min}$ the conductivity increases with decreasing T because of an increase in the number of clusters. At $T > T_{\min}$ the clusters dissociate upon heating, and we have $(d\sigma/dT)_p > 0$, as in an ideal plasma.

The value of v_0 can be extracted from measurements of the temperature coefficient of the conductivity. Figure 10 shows the density dependence of the temperature coefficient of the conductivity for mercury, $\Delta E = -2d \times (\ln\sigma)/d\beta$, extracted from measurements[66,67] of σ at $T = 1.025 T_c$. The "energy gap" $\Delta E(\rho)$ becomes equal to the ionization potential of the atom in the limit $\rho \to 0$; when the material is compressed, the gap narrows, disappearing at[2] $\rho \approx p_c$. Working from this condition and expression (18), we can rewrite the expression for $T_{\min}$ as

$$T_{\min}^{-1} = T_c^{-1} + g^{-1} \ln \frac{\rho_c}{\rho}. \tag{20}$$

At $p = 160$ bar this expression yields $T_{\min} = 2300$ K, and at $p = 20$ bar it yields $T_{\min} = 1400$ K, in satisfactory agreement with experiment. The pronounced "lowering" of the ionization potential in (18) makes it possible to describe the anomalously high conductivity in metal vapor.

These expressions give a qualitatively correct description of cluster effects. More-accurate models

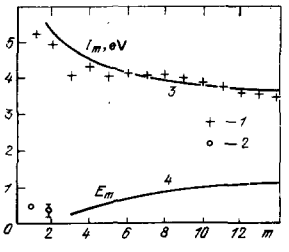

FIG. 9. I_m and E_m for the Na_m complex (in electron volts).[57] 1—Experiments of Ref. 76; 2—Na^- and Na_2^-; 3, 4—calculations.

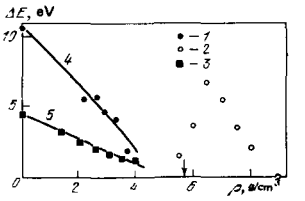

FIG. 10. "Transport gap" ΔE (4) and "optical gap" ΔE_{opt} (5) in mercury ($T \approx 1850$ K). Experimental data: 1—Ref. 66; 2—Ref. 67; 3—Ref. 68.

[1]The anomalously high binding energies predicted for negatively charged clusters Cs_m^- in Refs. 61 and 62 on the basis of the experimental results of Ref. 62 were not confirmed by subsequent measurements of the electrical conductivity[56,17,22] or calculations of the binding energy by the discrete-variational $X\alpha$ method.[63]

[2]There is an interesting point here: At $\rho > \rho_c$ the gap in mercury "opens up," while it closes at metallic densities. This anomalous feature occurs at $p \approx p_c$, but it disappears already at $p \gtrsim 2p_c$ (Ref. 94).

were developed in Refs. 69-71 and 57. In a calculation of the number of atoms in an ion cluster in Ref. 70, only the bound states, which apparently make the major contribution, were retained in the second virial coefficient for the ion–atom interaction. In this case we find

$$m = n\lambda^3 \frac{T^2}{2B\omega} e^{g/T}, \qquad (21)$$

where λ is the thermal wavelength, given by $\lambda = \sqrt{4\pi\hbar^2/MT}$; B is the rotational constant of the A_2^+ ion; ω is the vibrational quantum of this ion; and g is the binding energy of the atom in the ion, which is approximately equal to D_2^+ and also approximately equal to q, the latent heat of vaporization per atom.

A molecular-dynamics method was developed in Refs. 69, 72, and 73 for calculating the properties of nonideal plasmas. This method involves a computer simulation of the motion of a semiclassical electron in the field of scatterers. The electrical conductivity and thermoelectromotive force were calculated for mercury and cesium plasmas. The velocity autocorrelation function $\varphi(t) = \langle \mathbf{v}(0)\mathbf{v}(t)\rangle / \langle \mathbf{v}^2(0)\rangle$ contains the most comprehensive information on the electron dynamics. It follows from Fig. 11 that the electrons with positive energies are free, since $\varphi(t)$ falls off monotonically. With decreasing ε, a minimum ($\varphi < 0$) appears, since the electron does not immediately find its way through the complex potential field created by the atoms. Nevertheless, the autocorrelation time $\tau = \int_0^\infty \varphi(t)dt$ is not zero. These electrons are conduction electrons. Electrons with energies which are larger in magnitude but negative are localized in clusters ($\tau = 0$) and do not contribute to the static conductivity.

On the saturated-vapor line the number of particles in a cluster is highest, and the cluster may be regarded as a droplet of liquid metal stabilized by an ion.[71] In fact, the experimental results of Ref. 76 show that the ionization potential I_m of the Na_m complex and the electron affinity of this complex, E_m, are approximately equal to the work functions of neutral and negatively charged liquid-metal droplets. Specifically,

$$I(R) = I(\infty) + \frac{e^2}{2R}, \quad E(R) = E(\infty) - \frac{e^2}{2R}, \qquad (22)$$

where R is the droplet radius, determined by m and by the density of the liquid, n_L; $m = (4\pi/3)n_L R^3$; and $I(\infty) = E(\infty)$ is the work function of the metal. Large clusters thus become metallic, and we must abandon the approach based on a potential $V(r)$. For this reason, the parameters of the ionizational equilibrium are expressed in terms of the work function, the dielectric permittivity, and the surface tension in Ref. 71, as in the theory of heterogeneous nucleation.

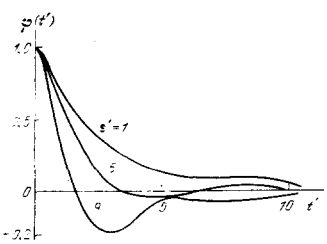

FIG. 11. Autocorrelation function $\varphi(t')$ in mercury. $n = 4.8 \cdot 10^{21}$ cm^{-3}; t' and $E = \varepsilon/g$ are the dimensionless time and energy.[72]

Figure 12 shows experimental results on the conductivity of a cesium plasma on the saturation line and on the isobar $p = 20$ atm obtained by heating in furnaces[54,55] and through the adiabatic compression of cesium vapor in a wind tunnel.[17,22] These measured conductivities are significantly higher than those predicted by the usual estimates for the saturated vapor based on the model of an ideal plasma ($\sigma = 10^{-5}$–10^{-4} mho/cm). The measured values correspond well to cluster models of plasmas.[69-71] Adiabatic-compression experiments[17,22] have raised the attainable plasma temperatures significantly and have made it possible to follow the disappearance of ion clusters as a result of their thermal dissociation.

At high pressures and temperatures, where experiments are very difficult, some really important information can be obtained by making a parallel study of two distinct kinetic coefficients. For example, the temperature dependence and the density dependence can be measured for the conductivity σ and the thermoelectric coefficient S. By definition, we have $J = \sigma(E + S\nabla T)$ in a nonuniformly heated material. In the experiments, measurements are taken of the potential difference which arises between the ends of an open circuit consisting of different conductors, whose junctions are at different temperatures. Figure 13 shows the results of measurements of the thermoelectromotive force. In an ideal plasma, the thermoelectromotive force and σ are related by $S = -(T/e)\mathrm{d}(\ln\sigma)/\mathrm{d}T$ (the relationship between S and σ in a nonideal plasma is slightly more complicated[74,75]). The supercritical isobars of S approach the ideal-gas dependence[3)] $S \approx I/2eT$, going through a minimum with $S_{min} \approx 10^{-3}\mu V/K$. This minimum is described in the model of Ref. 58 and is intimately related to the behavior of σ in (17) on supercritical isobars: $S = -(I - \Delta I)/2eT$. The supercritical isobars of S are described well by the results of the numerical simulation of Ref. 77, which used the same molecular-dynamics method as in the calculations of the electrical conductivity.

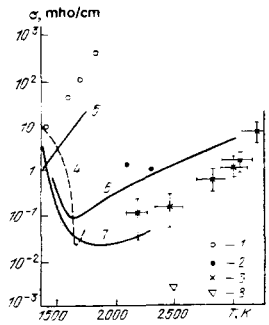

FIG. 12. Electrical conductivity of cesium vapor on the 20-bar isobar. Experimental data: 2—Ref. 55; 3—Ref. 22; 4—Ref. 54; 8—Ref. 21. Calculations: 6—Ref. 69; 7—Ref. 70. Electrical conductivity of saturated cesium vapor. 1—Experimental[55]; 5—calculated.[71]

[3)] In slightly nonideal cesium, with the predominant ion species Cs_3^+ and Cs^- ($p = 1$ bar), we have $S = -[I - (D_3^+ + D_2^+ - E)]/2eT$, where D_3^+, D_2^+, E are the binding energies of Cs_3^+, Cs_2^+, Cs^-.

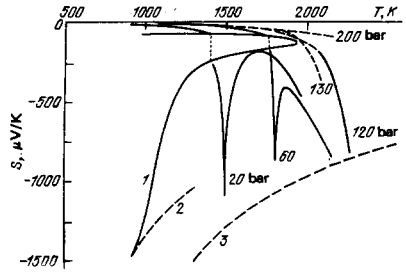

FIG. 13. Thermoelectromotive force of cesium. Experimental data: From Ref. 54 for $p = 20$, 60, and 120 bar; from Ref. 79 for $p = 130$ and 200 bar. 1—On the phase-equilibrium line; 2—$S = -[I - (D_3^+ + D_2^+ - E)]\,(2eT)^{-1}$; 3—$S = -I\,(2eT)^{-1}$.

For $p < p_c$ the S isobars behave in a more complicated way (going through two minima), not described by the theory. Here we need some more refined models. Apparently, as in an ideal plasma, the calculated values of the thermoelectromotive force are far more sensitive than the conductivity to the particular assumptions made. The situation is apparent from the experimental results on mercury[78]: Near the critical point, the S isobar crosses zero twice in a temperature interval $\Delta T = 50$ K.

4. ELECTRICAL CONDUCTIVITY OF A PLASMA WITH A HIGH DEGREE OF IONIZATION

At high temperatures the degree of ionization of a plasma increases. The Coulomb interaction between charged particles becomes predominant. The distinctive features of plasmas of different compositions are lost in the values of σ of a slightly nonideal plasma, and the pressure dependence weakens markedly, becoming manifested only through the dependence on the Coulomb logarithm. With increasing density in a nonideal plasma we find substantial deviations of the conductivity from that of a slightly nonideal plasma, as described by the Spitzer-Härm expression. In a very dense plasma, we begin to see the effect of the structure of the ion core.

The Spitzer-Härm expression[162] was extracted from a numerical solution of the Fokker-Planck equation:

$$\sigma_{Sp} = \gamma_E(z)\, 2\,(2T)^{3/2}\,(z\pi^{3/2}e^2m^{1/2}\ln\Lambda)^{-1}, \quad \ln\Lambda = \ln\frac{3}{\sqrt{2\Gamma}}, \qquad (23)$$

where z is the ion charge; for $z = 1$, incorporation of the electron–electron interaction yields $\gamma_E = 0.582$. In a partially ionized plasma, expression (23) is joined with the Lorentz expression for a weakly ionized plasma (in the usual way according to Ref. 80), so that the scattering of electrons by atoms can be taken into account:

$$\sigma = \frac{4}{3\pi}\frac{e^2}{mT^{3/2}}n_e\int_0^\infty d\varepsilon\, e^{-\beta\varepsilon}\varepsilon^{3/2}\Big[\nu_{ea}(\varepsilon) + \sum_j \gamma_E(z_j)\,\nu_{ej}(\varepsilon)\Big]^{-1}, \qquad (24)$$

where ν_{ea} and $\nu_{ej}(\varepsilon)$ are the rates at which electrons collide with atoms and with ions of charged z_j. In addition to the approach using expressions like (24), there is an effective variational method for calculating the conductivity of a partially ionized plasma.[81]

The Spitzer expression applies at small values of Γ, such that $\ln\Lambda \gg 1$. To calculate the corrections to (23) of higher order in Γ systematically is a complicated problem, solvable by perturbation-theory methods[82-84] which are applicable in the limit $\Gamma \ll 1$. A particular problem is to incorporate bound states in the quantum-mechanical kinetic equations.[103] Expression (23) and the expressions for the conductivity which follow from the asymptotic theories[82] do not have good extrapolation properties; they yield meaningless values of σ at $\Gamma \gtrsim 3/\sqrt{2}$. Consequently, several approaches based on models have been proposed to describe the deviations of the experimental values of the conductivity from (23). As in thermodynamics (Section 2), correct numerical simulations can be carried out here only for pseudopotential models which incorporate quantum-mechanical effects approximately along with the Coulomb interaction.[13]

The conductivity of dense plasmas measured in electric arcs, pulsed discharges, and shock waves agrees satisfactorily with the approximation of Refs. 162 and 82 at $\Gamma \lesssim 0.3$. At such small nonidealities, however, the question of just which of the electrons are conduction electrons becomes important, as in a weakly ionized plasma. Kakyugin and Norman[87] have suggested that the electrons which appear as a result of the lowering of the ionization potential (this means the electrons with energies $0 > \varepsilon > -\Gamma T$) are localized by density fluctuations and do not participate in the conduction. This suggestion was followed up in Ref. 95 by replacing n_e in expression (23) by the electron activity, $\xi = \lambda_e^{-3}\exp(-\beta\mu_e)$; the result was to improve significantly the extrapolation properties of the model at $\Gamma \gtrsim 1$.

Khomkin and Vorob'ev[86,88] have pointed out that electrons with small positive energies $\varepsilon < e^2/\bar{r} = \gamma T$ are also something less than totally free, interacting with ions, which localize near them. These electrons, in "collisional complexes," are distinguished from n_e, since the electron-ion complex is not, in a sense, a charged particle. As a result, at $\Gamma < 1$ the conductivity is found to be reduced by the decrease in the number of current carriers, $\sigma = \sigma_{Sp}(1 - 0.47\Gamma^{2/3})$, and the corresponding calculations agree well with experimental results in Ar, Cs, Xe, and H (Fig. 14).

Dynamic methods can be used to measure σ at $\Gamma \approx 0.3$-10 in plasmas of various chemical compositions,[92,56,47,93,95] approaching the degeneracy boundary

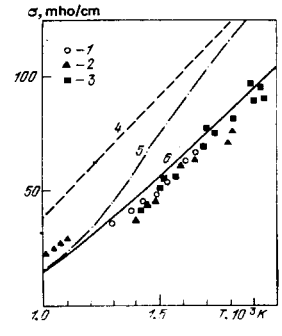

FIG. 14. Electrical conductivity of an argon plasma ($p = 150$ bar).[88] Experimental data: 1—Ref. 89; 2—Ref. 90; 3—Ref. 91. Theoretical results: 4—σ_{sp}; 5—Eq. (24); 6—Ref. 88.

of the electrons, $n_e\lambda_e^3 \approx 1$. For a comparison of the various results on σ, the component[4)] due to Coulomb collisions, σ_{Coul}, is singled out. The reduced conductivity $\sigma_{Coul}^* = \sigma_{Coul}(S_{Sp}\ln\Lambda)^{-1} = 0.98\gamma_E^{-1}ze^2m^{1/2}T^{3/2}$ is shown in Fig. 15. Comparing the results, we can clearly distinguish between "high-temperature" data (with $T \gtrsim 2 \cdot 10^4$ K) and "low-temperature" data.[95] The low-temperature ($T \lesssim 2 \cdot 10^4$ K) results obtained in various gases are in satisfactory agreement with each other, so that we can trace the effect of the Coulomb interaction over the entire range of parameters. The data of Ref. 20 depart slightly from the general trend in Fig. 15, apparently because of an overheating instability (Section 6) which occurs under these conditions. The results of Ref. 97 also depart slightly from the general trend.

The deviations of σ from σ_{Sp} become progressively larger with increasing Γ, and at $\Gamma \gtrsim 1$ expression (23) clearly becomes inapplicable. To describe the conductivity of a highly nonideal plasma, Gryaznov *et al.*[100] used a version of a method used for calculating σ in liquid metals and semiconductors: the Ziman approximation (Fig. 15). This approximation incorporates the ion-ion correlation,

$$\nu_{ej} = \frac{\sqrt{2}}{16\pi} n_j m^{-1/2}\varepsilon^{-3/2} \int_0^{4\varepsilon/e^2} |V_{ej}|^2 S_j(q)\, dq, \qquad (25)$$

where $V_{ej}(q)$ is the form factor of the potential, and $S_j(q)$ is a structure factor which reflects the ion–ion correlation. The quantity $4\varepsilon/e^2$, which limits the range of integration, provides the limiting transition of σ to σ_{Sp} at $\Gamma \ll 1$.

A systematic calculation of σ can be carried out by working from the solution of the kinetic equation for a nonideal plasma. Here the theory runs into serious difficulties, and progress has been slight. The Chapman-Enskog method was used in Ref. 82 to solve the Gould-Dewitt kinetic equation[82] with quantum diffraction and electron scattering by excited states in a pseudopotential approximation. This approach led to a good description of the results of dynamic experiments.[93,95] The expressions given for the conductivity in Ref. 102 incorporate quantum effects in the scattering by a screened (Debye) potential. Interesting results from a Green's-function calculation of the conductivity of a nonideal plasma were reported in Ref. 85; ion correlations, quantum effects, and static and dynamic screening were taken into account. The corresponding expression has the Spitzer asymptotic behavior in the limit $\Gamma \to 0$ and describes experimental results in the very nonideal region.

Measurements of the conductivity of a plasma[47,95] produced in explosive "cumulative" devices and behind shock waves reflected from condensed-matter obstacles indicate a disruption of the Coulomb behavior of the conductivity. The reason for the disruption of this "scaling" is that at high temperatures the Coulomb amplitude for the scattering of an electron by an ion, $f = e^2/T$, is comparable to the size of the ion (~4 Å for Xe+). At

[4)] Singling out the Coulomb component from the experimental results of Refs. 21 and 53 is a process afflicted with large errors, which in a number of cases reach values of several hundred percent.

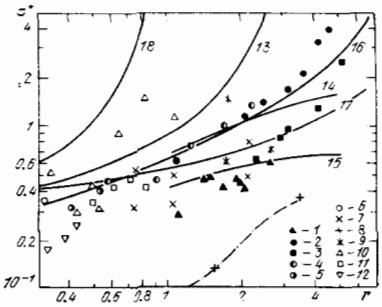

FIG. 15. Dimensionless conductivity of a nonideal plasma, σ^* (Ref. 95). Experimental data: 1, 2—Xe (Ref. 95); 3–6—Ref. 93; 3—Xe; 4—Ar; 5—Ne; 6—air; 7—Cs (Ref. 56); 8—Cs (Ref. 20); 9—Cs (Ref. 96); 10—Cu, air[97]; 11—Textolite[98]; 12—air.[99] Theoretical results: 13—Eq. (24); 14, 15—for $T = 20\,000$ K and 70 000 K, respectively[95]; 16—Refs. 47 and 100; 17—Ref. 101; 18—for $n_e = 10^{21}$ cm^{-3} (Ref. 82).

these distances the potential $V_{ej}(r)$ becomes stronger than the external Coulomb potential. The effect is to increase the rate of electron-ion collisions, ν_{ej}, and thus lower the plasma conductivity. The following pseudopotential[104] was used in Ref. 95 to incorporate these aspects of the electron–ion scattering at high electron energies:

$$V_{ej}(r) = -e\left[\frac{z_j}{r} + (z - z_j)\frac{\exp(-\beta r)}{r}\right]\exp\left(-\frac{r}{r_D}\right),$$
$$\beta = 1.8 z^{1/3}(z - z_j)^{-1}a_0^{-1}. \qquad (26)$$

In the limit $r \to 0$, $V_{ej}(z)$ becomes the Thomas-Fermi potential, while in the limit $r \to \infty$ it becomes the Debye potential. Curves 15 and 14 in Fig. 15 are plotted from (26) with $n_e = \xi$. The calculated results give a good description of the stratification of the isotherms of the reduced electrical conductivity of a nonideal plasma.

5. OPTICAL PROPERTIES

The effect of a slight nonideality on the optical properties of a plasma is well known.[105] The effect can be summarized as a broadening of the spectral lines and a shift of the photoionization thresholds. With increasing nonideality, some distinctive new phenomena occur in the plasma as a result of changes in the structure and in the energy spectrum. At low temperatures in a weakly ionized plasma, the changes are primarily the "closing of the optical gap" and low-frequency cluster absorption.

The optical properties of mercury were measured in Refs. 106-108 in experiments on reflection and transmission. At high densities, $\rho \gtrsim 9$ g/cm^3, the optical properties are typical of the liquid-metal state. As ρ decreases, some qualitatively new effects appear. The curve of the absorption coefficient $K(\omega)$ in Fig. 16 shows two distinctive features: a sharp edge of a broad absorption band, which shifts in the red direction with increasing ρ, and a low-frequency plateau.

It can be assumed[109] that the edge is the tail of a band which appears upon transitions from the ground state of mercury atoms to exciton states, which are the result of an evolution of the 6*p* level. The absorbing atom is surrounded closely by atoms (a neutral cluster), and the absorption coefficient is $K(\omega) \sim \rho(\omega)$, where $\rho(\omega)$ is the electron state density in the excited cluster.[110,111] In a first approximation we can write

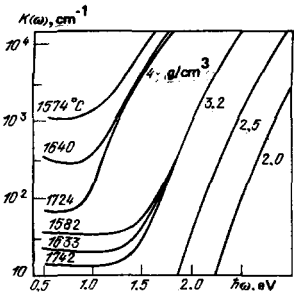

FIG. 16. Optical absorption coefficient of mercury.[112]

$$\rho(\omega) \sim \exp\left(-\frac{\hbar\omega - \Delta E_{opt}}{\Delta E_t^2}\right), \qquad (27)$$

where ΔE_{opt} is the "optical gap," equal to the excitation energy of the atom in the limit $\rho \to 0$, and ΔE_t is the band half-width. Estimates in Refs. 110 and 111 yielded reasonable values for ΔE_{opt} and ΔE_t. The gap ΔE_{opt} decreases with increasing ρ and, like the transport gap ΔE, disappears at $\rho \approx \rho_c$. We see that the insulator–metal transition which occurs during the compression of the plasma is manifested in not only the electrical properties but also the optical properties.

For a long time the plateau at low frequencies went unexplained. Further measurements finally led to the conclusion[112] that the plateau results from the absorption of light by charged clusters. In Fig. 17, from Ref. 12, we can see an absorption band which creates a plateau. On the plateau the coefficient $K(\omega)$ increases with increasing ρ and with decreasing T. The cluster density n_m behaves in the same way. It is possible that the plateau results from the photodetachment of an electron from an electron cluster.

Optical absorption by charged clusters was first discussed in Ref. 65 on the basis of a classical model for the highfrequency conductivity $\sigma(\omega)$, with $K(\omega) \sim \sigma(\omega)$. The conclusions of Ref. 112 were based directly on the results of Ref. 73, where $\sigma(\omega)$ was calculated by methods which had been used previously to calculate the electrical conductivity and thermoelectromotive force of mercury and cesium plasmas. There is qualitative agreement between theory and experiment.

There is, however, the possibility that the clusters become metallic at high densities, as mentioned in Section 3. If so, a different approach should be taken to describe the interaction of light with clusters.

At high temperatures the optical properties of a plasma with a high degree of ionization are significantly affected by the Coulomb nonideality.[113,117] The very first experiments carried out at $\Gamma \lesssim 0.3$ and $n_e \lesssim 10^{18}$ cm^{-3}, which were slightly contradictory, revealed that the emission in the continuum was slightly more intense than predicted by the calculations (Fig. 18). At large nonidealities, on the other hand, the intensity of the emission near the photoionization thresholds is much weaker than predicted by conventional calculations.[105] This effect has recently attracted considerable interest.

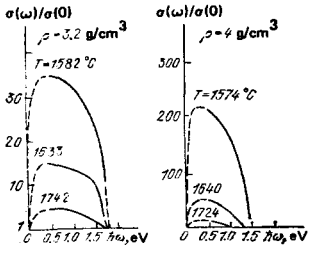

FIG. 17. The ratio $\sigma(\omega)/\sigma(0)$ of dense gaseous mercury at various temperatures and densities.[112]

According to the standard interpretation,[105] the effect of the plasma interaction reduces to a broadening of lines and a shift of the photoionization boundary. As a result, there is a significant increase in the optical absorption coefficient in the threshold region of the spectrum. Fluctuating microscopic fields $\bar{E}$ cause a distortion of the intraatomic potential at large distances in the energy range $\Delta\varepsilon(\bar{E}) = 2e\sqrt{e\bar{E}} \sim \gamma T$. It was suggested in Refs. 117 and 119 that the electron state density $\rho(\varepsilon)$ is approximately classical at $\varepsilon < 0$ but shifted by an amount $\Delta\varepsilon$ (Fig. 19). If the perturbation of the wave functions is assumed small in the evaluation of the matrix element for an optical transition, the use of $\rho(\varepsilon)$ from Fig. 19 leads to a dip in the distribution of the oscillator strength density near the threshold. This effect means that a transparency window appears in the spectrum as Γ increases. These ideas were used in Ref. 120 to interpret the emission spectra of mercury plasmas, and it was noted that several spectral lines were missing.

Regardless of the description method (fluctuating microscopic fields[120] or plasma screening[121-123]), it is natural to expect that the interparticle interaction will lead to a shorter-range potential in a dense plasma, changing the energy spectrum of electrons bound in atoms and ions. We do not yet have a systematic description of the observed effects, and experiments have not yet been carried out over the entire range of conditions.

Direct calculations of the oscillator strength density were carried out in Ref. 124 through a numerical solu-

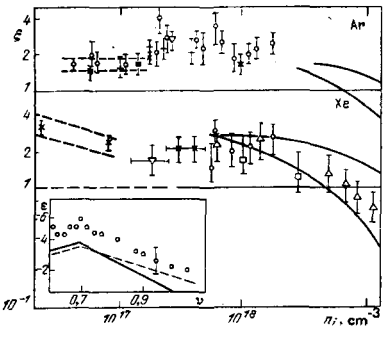

FIG. 18. Density dependence[117] of the ratio of the experimental and theoretical[105] values of the absorption coefficient, $\xi = \varkappa_{expt}(\nu)/\varkappa_{theo}(\nu)$, for argon ($\nu = 6.66 \cdot 10^{14}$ s^{-1}) and xenon [$\nu = (6.6\text{–}6.9)\ 10^{14}$ s^{-1}] plasmas; and also the emissivity ε [in units of 10^{-12} W/(cm^3 · s · sr)] of an argon plasma (p = 10 atm, T = 14150 K) as a function of the frequency (in units of 10^{15} s^{-1}). 1—Theoretical[105]; 2—Ref. 118 (see Ref. 117 for the detailed notation).

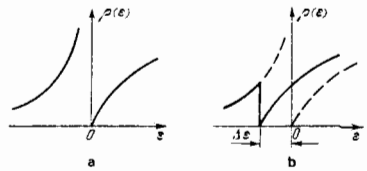

FIG. 19. Density of electron states, $\rho(\varepsilon)$, in low-density (a) and dense (b) plasmas.[119]

tion of the Schrödinger equation for a Debye potential and for a "bounded" Coulomb potential. The transparency window was not found there, in calculations for a hydrogen plasma. Careful experiments on the emission of hydrogen in the threshold region of the spectrum were carried out in a shock tube in Ref. 125 ($n_e \approx 8 \cdot 10^{17}$ cm^{-3}) and in a discharge apparatus in Ref. 126 [$n_e = (2\text{-}6) \cdot 10^{17}$ cm^{-3}; Fig. 20]. These experiments revealed no effects which might have been caused by a dip in the distribution of the oscillator strength density. The emission spectrum had the usual shape[105] with a shifted photoionization boundary. It is possible, however, that the new effects expected in a hydrogen plasma will appear at even higher values of Γ; further experiments are required to resolve this question.

The most regular effects of nonideality were found in argon,[116] in a study carried out over a broad range of parameters, from $n_e \approx 10^{18}$ cm^{-3}, $\Gamma \approx 0.3$ to $n_e \approx 2 \cdot 10^{20}$ cm^{-3}, $\Gamma \approx 1.6$. Similar effects were subsequently observed in xenon.[127,128]

A pronounced nonideality changes the emission characteristics of an argon plasma ($T = 2 \cdot 10^4$ K; Fig. 21). The experimental data for low densities agree with the results of numerous earlier measurements (Fig. 18) and confirm the tendency for the experimental emission to exceed the calculated emission. As the plasma is compressed further, the specific absorption coefficient $k(\omega)/n$ falls off monotonically, remaining nearly an order of magnitude below the predictions of the conventional plasma calculations[105] (the $bf + ff$ curve) and close to the values determined exclusively by free-free transitions (the ff curve). In an intraatomic potential bounded by an interparticle interaction the number of discrete energy levels is finite because highly excited states move into the continuum.

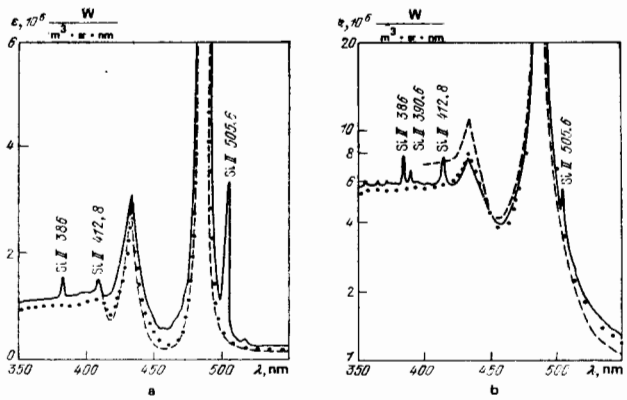

FIG. 20. Emission spectrum of a hydrogen arc.[126] a—$p = 0.45$ bar, $T = 1300$ K, $n_e = 2.2 \cdot 10^{17}$ cm^{-3}; $p = 7.2$ bar, $T = 15200$ K, $n_e = 6 \cdot 10^{17}$ cm^{-3}. Solid curves—Experimental; dashed curves—theoretical[129]; dotted curves—theoretical[129] with line overlap and a shift of the Balmer continuum; Si II—lines of a silicon impurity.

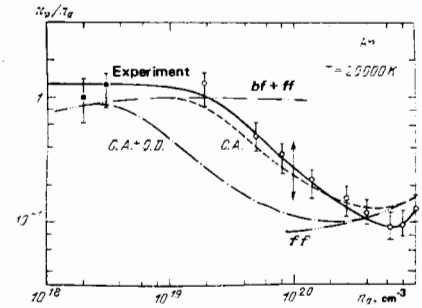

FIG. 21. The specific absorption coefficient of an argon plasma, $\varkappa_\nu/n$, as a function of the density of absorbing atoms.[116] $\nu = 5.2 \cdot 10^{14}$ s^{-1}. Circles—Experimental; ff—free-free transitions; $bf + ff$—photoionization added to free-free transitions; $CA + QD$—model of a "bounded atom"[41] with the shifted photoionization cross sections from Ref. 118; CA—calculation from the complete model of a bounded atom.

Bespalov *et al.*[116] used the model of a bounded atom, discussed in Section 2 in connection with the interpretation of thermodynamic measurements, to generate a qualitative description of level deformation. This model can be used to determine the positions of atomic energy levels and to calculate the photoionization cross sections of atoms, with allowance for the effect of the discrete and continuous spectra of the plasma particles on the wave functions (Fig. 22). The resulting curve of the absorption coefficient as a function of the compression is shown in Fig. 21 (curve C.A.). As the plasma is compressed, some of the excited energy levels are pushed into the continuum, so that photoionization absorption of these excited states is eliminated.

6. DYNAMICS OF A NONIDEAL PLASMA AND STABILITY IN EXTERNAL FIELDS

The physical properties of nonideal plasmas have several interesting qualitative consequences when external electric and magnetic fields and also pressure gradients are imposed. The first observation of such effects was in Ref. 20. A cesium wire was heated by a current in an argon atmosphere in such a manner that the resulting plasma column expanded over time. Significantly, the plasma became stratified in the direction perpendicular to the current flow, breaking up into a large number of regularly alternating dark and bright layers. It was shown in Ref. 130 that an overheating instability occurs in the resulting nonideal plasma and causes this stratification.

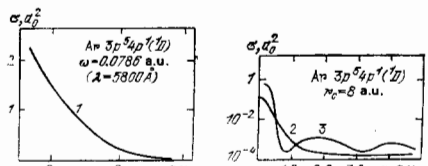

FIG. 22. Photoionization cross section of argon as a function of the degree of plasma compression (1) and of the frequency (2) at a fixed compression in the momentum representation (3—"isolated atom").

When a substance is heated on a supercritical isobar, a metal–insulator transition takes place. The conductivity falls off during the heating, $d\sigma/dT<0$ (Fig. 6). If the current (i) heating the material is stabilized (if there is a large resistance in the external circuit), then small temperature fluctuations $\delta T>0$ cause an unbounded growth of the Joule heat evolution i^2/σ.

The basic system of equations consists of the mass balance equation, Ohm's law, the field equations, and the heat-balance equation,

$$\frac{C_p\,dT}{dt}=\frac{i^2}{\sigma s^2},$$

where C_p is the heat capacity, and s is the cross-sectional area of the plasma column. The growth rate of the overheating instability, γ, is inversely proportional to the heating scale time $t_h=C_pT/(i^2\sigma^{-1}s^{-2})$, and is given approximately by

$$\gamma=-t_h^{-1}\left(\frac{d\ln\sigma}{dT}\right)_p. \tag{28}$$

Large absolute values $|d(\ln\sigma)/dT|$ lead to high perturbation growth rates. It is shown in Ref. 130 that the fluctuations which grow most rapidly give rise to layers which are oriented perpendicular to the current and which may be called "thermal" striations.

The appearance of inhomogeneities affects the average plasma properties found experimentally. The steady states of a plasma column heated by a current and bounded by walls were studied in Ref. 131. Curves of $\sigma(T,p)$ modeling the nonmonotonic behavior actually observed, shown in Fig. 6, were used. As a result, the voltage-current characteristics of the plasma column were found to have descending branches, which resulted in inhomogeneities of the current-heated plasma. There is the question of how the intrinsic plasma conductivity $\sigma(T)$ is related to the measured average value $\sigma_{eff}=\bar{i}/s\bar{E}$, where $\bar{i}$ and $\bar{E}$ are the measured (average) values of the current and the electric field. It is shown in Ref. 131 that if an isobar has a narrow minimum the $\sigma_{eff}(T)$ curve will have some new qualitative features in an inhomogeneous plasma. The $\sigma_{eff}(T)$ isobar passes through a minimum, increases, and reaches a maximum at a certain T_{max}. At $T>T_{max}$, therefore, σ_{eff} (in contrast with σ) decreases with increasing T (Fig. 23). This effect must be kept in mind in interpreting the measurements of $\sigma_{eff}(T)$ during Joule heating.

The experiments of Ref. 20, discussed in Section 4, revealed a descending region on the temperature dependence of the conductivity, at $T=10^4$–$2\cdot10^4$ K. In light of the discussion above, it seems highly likely that this anomaly was caused by an inhomogeneity of the plasma column.

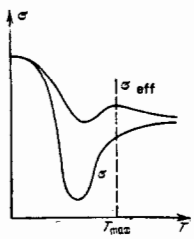

FIG. 23. Temperature dependence of the true, $\sigma(T)$, and measured, $\sigma_{eff}(T)$, electrical conductivities of an inhomogeneous plasma.[131]

The particular behavior of the thermal conductivity of a nonideal plasma may also have some interesting consequences. While the electrical conductivity of a plasma, σ_{pl}, is low in comparison with the electrical conductivity of a metal, σ_M, at $T_{pl}\approx10^4$ K, the thermal conductivity λ_{pl} may exceed λ_M. The reason lies in the important role played by radiative heat transfer, $\lambda_{pl}\approx\lambda_R$ (the radiative thermal conductivity λ_R was studied in Ref. 134). This circumstance may result in the propagation of a narrow temperature front during isobaric Joule heating of a liquid metal in a capillary.[132] At the front of this wave, propagating at a velocity u through the metal, the material goes from a metallic state to a plasma state.

The structure of the front (Fig. 24) is determined by the solution of the energy balance equation. In the coordinate system in which the front is at rest, we have

$$\frac{d[\lambda(T)\,dT/dx]}{dx}-\frac{u_m\rho_m\,dT}{dx}+\frac{i^2}{s^2\sigma(T)}-F(T)=0, \tag{29}$$

where ρ_m is the density of the liquid, u_m is the velocity at which the liquid is flowing in at the front, $s=\pi R^2$, R is the radius of the capillary, and $F\approx-R^2\int_0^T\lambda(T')dT'$ is the heat loss at the capillary wall. The propagation of the front is analogous to the propagation of a slow-flame front.[135] In the presence of two phases (hot and cold) the thermal conductivity warms the cooler regions, reducing σ and causing intense heat evolution there. The result is a wavelike propagation of the hot phase, with heat evolution localized at the wavefront. The expression $u_M\approx\lambda_R/C_p\rho_MR$ was derived in Ref. 132 for the wave velocity. A wave of this type was apparently observed in cesium in Ref. 133. At $p=500$ bar and $i/s=10^4$ A/cm^2 the wave velocity was $u=2u_M\rho_M/\rho\approx10$ m/s.

Dissociation and ionization cause the viscosity coefficient and the thermal conductivity to vary rapidly and nonmonotonically as functions of the temperature (Fig. 25). This circumstance may cause a qualitative change in the viscous flow of a plasma in the channels of MHD generators,[3] the heat-evolution elements of nuclear reactors,[2] technological plasma-chemistry apparatus,[10] and other systems. The viscous dissipation of energy under conditions of limited heat removal results in a significant temperature rise, reducing the viscosity and causing an "explosive" acceleration of the flow.

"Hydrodynamic" explosion conditions were analyzed in Ref. 136, where the temperature dependence of the thermal conductivity was taken into account, in contrast

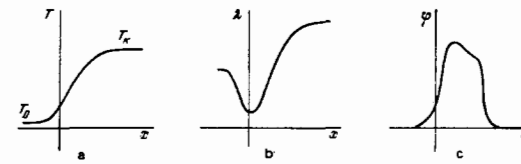

FIG. 24. Distributions of the temperature (a), the thermal conductivity λ(b), and the heat evolution $\varphi=(i^2/s^2\sigma-F)$ (c) at a heating wavefront in cesium.[132]

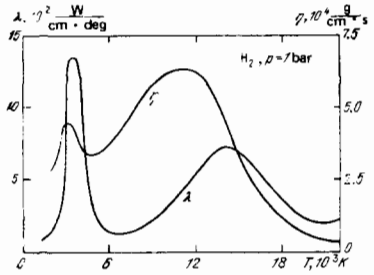

FIG. 25. Temperature dependence of the viscosity and thermal conductivity of a hydrogen plasma.

with the conventional analysis approach.[137] A study was made of the one-dimensional steady-state viscous flow of a plasma between plates with T_0 = const under the influence of a constant pressure gradient $b = -\partial p/\partial z$ along the z axis. The equation of motion, the energy equation, and the boundary conditions for this type of flow are

$$\frac{\partial}{\partial x}\left(\eta\frac{\partial v}{\partial x}\right)-\frac{\partial p}{\partial z}=0,\quad \frac{\partial}{\partial x}\left(\lambda\frac{\partial T}{\partial x}\right)+\eta\left(\frac{\partial v}{\partial x}\right)^2=0, \qquad (30)$$
$$v'(0)=T'(0)=0,\quad v(x_0)=0,\quad T(x_0)=T_0,$$

where η and λ are the shear viscosity and the thermal conductivity, and x_0 is the distance between the plates. For the case of intense dissociation or ionization of the plasma the following assumptions were adopted:

$$\eta=\eta_0\, e^{E_1/kT},\quad \lambda=\lambda_0 e^{E_2/kT}. \qquad (31)$$

Table I shows some representative values of η_0, λ_0, E_1, and E_2 for cesium and potassium plasmas near T = 2000 K and p = 0.1 bar. Analysis of solution (30) and of its stability with respect to one-dimensional perturbations has shown[136] that in the case of an exponentially increasing thermal conductivity, $E_2>0$, the explosive regime sets in for planar flow under the condition $K>K_{cr}\approx 16E_1/E_2$, while for axisymmetric flow it sets in under the condition $K>K_{cr}\sim 10^2E_1/E_2$, where $K=b^2x_0^4E_1e^{(E_2-E_1)/kT}/\lambda_0\eta_0T_0^2$. In a study of the flow of hotter and denser plasmas ($T\gtrsim 10\,000$ K, $p\gtrsim 10$ atm), the boundary conditions on the temperature should be changed, and radiative heat transfer should be taken into account (in the approximation of radiant heat conductivity, for example). The coefficient of radiative heat transfer changes even more rapidly than λ with temperature, thus favoring the conditions for a hydrodynamic explosion in the plasma.

In the analysis of hydrodynamic phenomena in a superdense plasma produced by a pulsed local concentration of energy one must not ignore the possible appearance of phase stratification regions. Differential expressions for the slopes of the plasma isentropes and isotherms in single-phase and two-phase regions were derived in Ref. 139 for an equation of state of a general type on the basis of thermodynamic identities and the phase-equilibrium conditions. That analysis[139] showed (Fig. 26) that the possibility of a phase transition during an adiabatic change in the pressure in the plasma is determined by the modulus of the isothermal expansion of the original phase, $(\partial V/\partial T)_p$, and by the properties of the interface, dT/dp and dS/dT. A corresponding analysis was carried out in Refs. 139-141 for shock-compression conditions. The structure of the compression and rarefaction waves in media with an arbitrary equation of state was analyzed in Refs. 142-144. The structure is determined by the sign of the derivative $(\partial^2 p/\partial V^2)_s$, which can become negative as a result of plasma phase anomalies. In this case the flow breaks up into several shocks (Fig. 27) separated by smooth compression waves. During the expansion of the plasma, rarefaction shock waves form, similar to those observed in the elastoplastic region[145] and near the critical point of Freon.[146] These qualitative hydrodynamic phenomena may be manifested in experiments on the excitation of ultrahigh pressures accompanied by shock waves and rarefaction waves.

A problem of special interest is the stability of shock waves in plasmas where dissociation and ionization occur.[134] The stability of steady-state plane shocks with respect to slight periodic perturbations of the front was studied in Ref. 147 and later in Refs. 148–151, where the following conditions were formulated:

$$\left(\frac{\partial V}{\partial p}\right)_H<\frac{V_0-V}{p-p_0}, \qquad (32)$$

$$\left(\frac{\partial V}{\partial p}\right)_H>\frac{V_0-V}{p-p_0}\left(1+2\frac{V}{V_0}\frac{D}{c}\right),\quad c=\sqrt{-V^2\left(\frac{\partial^2 p}{\partial V^2}\right)_S}, \qquad (33)$$

$$\frac{V_0-V}{p-p_0}\,\frac{1-\frac{V^2}{V_0^2}\left(\frac{D}{c}\right)^2-\frac{V}{V_0}\left(\frac{D}{c}\right)^2}{1-\frac{V^2}{V_0^2}\left(\frac{D}{c}\right)^2+\frac{V}{V_0}\left(\frac{D}{c}\right)^2}<\left(\frac{\partial V}{\partial p}\right)_H<\frac{V_0-V}{p-p_0}\left(1+2\frac{V}{V_0}\frac{D}{c}\right). \qquad (34)$$

Conditions (32) and (33) correspond to an absolute instability of the shock wave. Condition (32) leads to a flow pattern[142] (which has been studied well, both theoretically and experimentally) containing several shocks separated by continuous compression waves (Fig. 27). Analysis shows that condition (33) is difficult to satisfy in practice. This condition is more stringent than the condition

$$\left(\frac{\partial V}{\partial p}\right)_H>\frac{V_0-V}{p-p_0}, \qquad (35)$$

TABLE I.

Element	η_0	λ_0	E_1	E_2	x_0	b	R_e	$\frac{C_p\eta_0}{\lambda_0}$
K	$1.28\cdot10^{-4}$	$1.47\cdot10^{5}$	$0.88\cdot10^{-12}$	$0.84\cdot10^{-12}$	1.0	$0.704\cdot10^{3}$	$2.05\cdot10^{3}$	10^{-2}
Cs	$1.98\cdot10^{-5}$	$4.17\cdot10^{5}$	$1.678\cdot10^{-12}$	$1.63\cdot10^{-12}$	1.0	$3.91\cdot10^{2}$	$2.8\cdot10^{3}$	10^{-3}

cgs electrostatic units

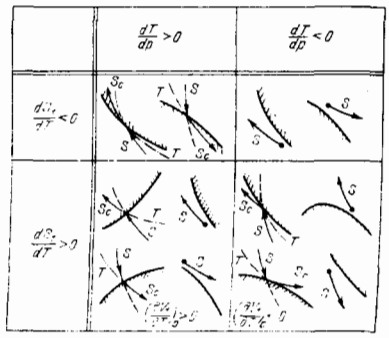

FIG. 26. Possible situations near the phase boundaries (hatching) for isothermal (T) and adiabatic (S) pressure changes in a plasma. s_c—Isentrope of the two-phase region.

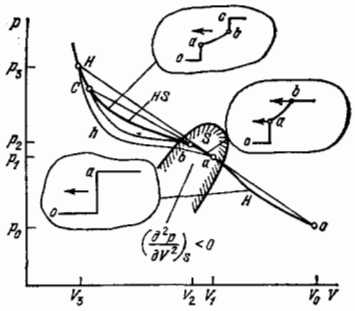

FIG. 27. Wave adiabatic in a medium with the sign of $(\partial^2 p/\partial V^2)_s$ capable of being positive or negative. The insets show the longitudinal profiles of the density of the shock wave corresponding to the various regions of the wave adiabatic.

which corresponds to single-valuedness of the shock compression.[152,153]

The region defined by condition (32) is apparently the region of the most practical interest in plasma physics, since there is the hope that we can actually satisfy this condition experimentally. Condition (34) determines the region of "spontaneous emission of sound by a shock," in which perturbations are of the form of undamped traveling waves which are propagating along the direction of the shock, lagging behind it as time passes. A nonlinear analysis of this situation was carried out in Ref. 154. The region of the return branch of the shock adiabatic, $(\partial p/\partial V)_H > 0$, is also attractive for satisfying the condition for the "acoustic" instability, (34). This form of the Hugoniot adiabatic in the pV plane is typical[142] of plasmas in which internal degrees of freedom (ionization; dissociation; vibrational, rotational, and electronic excitation; etc.) are excited as the temperature is increased. Figure 28 shows shock adiabatics of a superdense tungsten plasma, H_{TF}, from Ref. 155, calculated from the approximate expressions of the semiclassical Thomas-Fermi theory.[156] The wavy curve in Fig. 28 is the lower boundary of the instability region corresponding to (34), while the upper boundary lies outside the range of applicability of the semiclassical model, by virtue of the spontaneous creation of electron–positron pairs in such a plasma.[157] Incorporating the energy of the equilibrium-radiation pressure (H_1) makes the shock compression stable over the entire pressure range.

Figure 29 shows shock adiabatics of a two-phase mix-

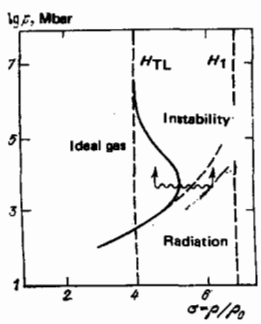

FIG. 28. Shock adiabatic of tungsten at ultrahigh pressures.[155] The wavy line shows the instability region, (34).

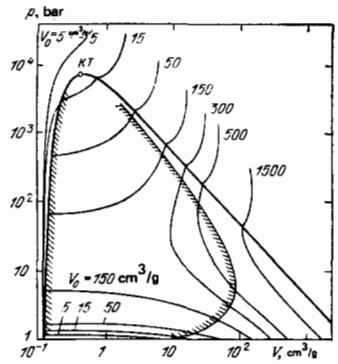

FIG. 29. Shock adiabatics of copper in the boiling region calculated from the equation of state.[34] Hatching—instability region, (32); solid curve—phase boundary. The labels on the shock adiabatics are the initial specific volumes in units of cubic centimeters per gram.

ture of a liquid and a metal vapor according to calculations from the semi-empirical equation of state for copper.[34] The return branch of the shock adiabatics and the resulting acoustic instability, (34), are determined by phase conversions. The slope changes caused on the shock adiabatics by thermal ionization are particularly significant for nonideal cesium plasmas,[159] since the first and second ionization potentials are very different in this case (3.89 and 25.1 eV). Figure 30 shows shock adiabatics calculated for a cesium plasma in the ring approximation in a grand canonical ensemble.[159] The thermodynamic measurements of Ref. 19 yielded a plasma compressibility which is lower than predicted in Ref. 159 and which causes a slight shift of the acoustic-instability boundary in Fig. 30 toward higher pressures.

In some recent interferometric measurements[160,161] of the compression of gaseous Ar, Xe, and CO_2 by plane shock waves, instabilities were observed in the plasma behind the wavefront. The observed effects were attributed there to the return branch of the shock adiabatics, although in none of the cases studied was the condition for the acoustic instability, (34), satisfied. It may be that the inhomogeneities observed in Refs. 160 and 161 resulted from kinetic effects during plasma dissociation and ionization.

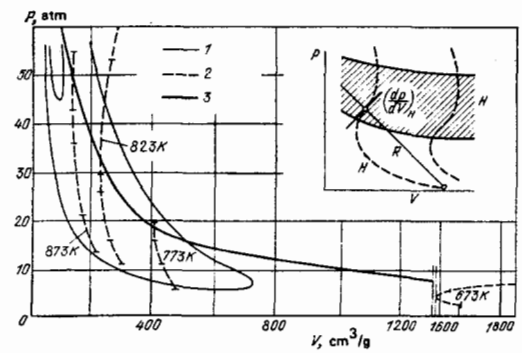

FIG. 30. Shock adiabatics of a cesium plasma.[158] 1—Curves of $\Gamma = e^2/Tr_D = \text{const}$; 2—Hugoniot adiabatics (labeled with the initial temperatures); 3—stability boundary according to (34). The inset at the upper right is a schematic diagram of the shock adiabatics and of the instability region (hatched) at high pressures.

7. CONCLUSION

High-pressure plasmas constitute one of the most rapidly growing fields of plasma physics. At this point, ideas are crystallizing on the thermodynamics and electrical conductivity (but not the optical properties!) in the region accessible to static experiments ($T \lesssim 3000$ K). Systematic research, however, will apparently have to await the powerful impetus of applications, as in other fields of plasma physics. At very high pressures ($p \gtrsim 1$ kbar), accessible only to dynamic experiments, we have so far seen only some pioneering studies. Interest in this region has recently picked up greatly.

Although it is difficult to push the theory far beyond experiment in the region of pronounced nonideality, definite progress has been made. This progress has taken the direction of the development of new quasiparticle models for electrons, atoms, and ions. These models can be used for computer simulations of the state of nonideal plasmas.

It is fair to say that research on the optical properties is still lagging behind, although there has been progress in recent years. Research on the dynamics and stability of nonideal plasmas is only beginning. There is definite hope that some interesting new effects will be found here.

[1]A. M. Prokhorov, S. I. Anisimov, and P. P. Pashinin, Usp. Fiz. Nauk **119**, 401 (1976) [Sov. Phys. Usp. **19**, 547 (1976)].
[2]V. K. Gryaznov *et al.*, Teplofizicheskie svoĭstva rabochikh sred yadernoĭ énergeticheskoĭ ustanovki s gazofaznym reaktorom (Thermophysical Properties of the Working Media of Nuclear Power Plants with Gas-Phase Reactors), Atomizdat, Moscow, 1980.
[3]L. M. Biberman, A. A. Likal'ter, and I. T. Yakubov, Teplofiz. Vys. Temp. **20**, 565 (1982).
[4]V. A. Alekseev, A. A. Vedenov, L. S. Krasitskaya, and A. N. Starostin, Pis'ma Zh. Eksp. Teor. Fiz. **12**, 501 (1970) [JETP Lett. **12**, 351 (1970)].
[5]V. E. Fortov, Dinamicheskie metody v fizike plazmy (Dynamic Methods in Plasma Physics), IKhF Akad. Nauk. SSSR, Chernogolovka; Usp. Fiz. Nauk **138**, 361 (1982) [Sov. Phys. Usp.
[6]P. Caldirola and H. Knoepfel (editors), Physics of High Energy Density, Acad. Pr. (1971) (Russ. Transl. Mir, Moscow, 1974).
[7]C. E. Ragan *et al.*, J. Appl. Phys. **48**, 2860 (1977).
[8]W. Ebeling, W. D. Kraeft, and D. Kremp, Theory of Bound States and Ionizational Equilibrium in Plasmas and Solids (Russ. Transl. Mir, Moscow, 1979).
[9]L. P. Kudrin, Statisticheskaya fizika plazmy (Statistical Plasma Physics), Atomizdat, Moscow, 1974.
[10]L. S. Polak (editor), Ocherki fiziki i khimii nizkotemperaturnoĭ plazmy (Essays on the Physics and Chemistry of Low-Temperature Plasmas), Nauka, Moscow, 1971.
[11]V. A. Alekseev, A. A. Andreev, and M. V. Sadovskiĭ, Usp. Fiz. Nauk **132**, 47 (1980) [Sov. Phys. Usp. **23**, 551 (1980)].
[12]A. G. Khrapak and I. T. Yakubov, Élektrony v plotnykh gazakh i plazme (Electrons in Dense Gases and Plasmas), Nauka, Moscow, 1981.
[13]B. V. Zelener, G. É. Norman, and V. S. Filinov, Metod Monte-Karlo v statisticheskoĭ fizike (The Monte Carlo Method in Statistical Physics), Nauka, Moscow, 1976.
[14]R. G. Ross and D. A. Greenwood, Prog. Mater. Sci. **14**, 173 (1971).
[15]V. A. Alekseev, V. G. Ovcharenko, and Yu. F. Ryzhkov, J. Phys. (Paris) **41**, 8, Suppl. C8-82, 1980.
[16]A. G. Kunavin *et al.*, Teplofiz. Vys. Temp. **11**, 261 (1973).
[17]I. M. Isakov and B. N. Lomakin, Teplofiz. Vys. Temp. **17**, 262 (1979).
[18]B. N. Lomakin and V. E. Fortov, Zh. Eksp. Teor. Fiz. **63**, 42 (1972) [sic].
[19]V. V. Bushman *et al.*, Zh. Eksp. Teor. Fiz. **69**, 1624 (1975) [Sov. Phys. JETP **42**, 828 (1975)].
[20]I. Ya. Dikhter and V. A. Zeĭgarnik, Teplofiz. Vys. Temp. **15**, 471 (1977).
[21]N. V. Iermokhin *et al.*, J. Phys. (Paris) **39**, 5, Suppl. C1-200 (1978).
[22]B. N. Lomakin and A. D. Lopatin, Teplofiz. Vys. Temp. **21**, No. 1 (1983).
[23]E. Wigner, Trans. Faraday Soc. **4**, 678 (1938).
[24]G. Carmi, J. Math. Phys. **9**, 2120 (1968).
[25]D. Caprley, Phys. Rev. **B18**, 3126 (1978).
[26]G. É. Norman and A. N. Starostin, Teplofiz. Vys. Temp. **8**, 413 (1970).
[27]M. Baus and J. P. Hansen, Phys. Rep. **59**, 1 (1980).
[28]A. G. Khrapak and I. T. Yakubov, Zh. Eksp. Teor. Fiz. **32**, 514 (1971) [*sic*].
[29]L. D. Landau and Ya. B. Zel'dovich, Zh. Eksp. Teor. Fiz. **14**, 32 (1944).
[30]D. A. Kirzhnits, Usp. Fiz. Nauk **119**, 357 (1976) [Sov. Phys. Usp. **19**, 530 (1976)].
[31]O. V. Dolgov and E. G. Maksimov, Usp. Fiz. Nauk **135**, 441 (1981) [Rev. Mod. Phys. **53**, 81–93 (1981)].
[32]I. K. Kikoin *et al.*, Zh. Eksp. Teor. Fiz. **49**, 124 (1965) [Sov. Phys. JETP **22**, 89 (1966)].
[33]V. E. Fortov, A. N. Dremin, and A. A. Leont'ev, Teplofiz. Vys. Temp. **13**, 1072 (1975).
[34]L. V. Al'tshuler *et al.*, Zh. Eksp. Teor. Fiz. **78**, 741 (1980) [Sov. Phys. JETP **51**, 373 (1980)].
[35]J. W. Shaner and G. R. Gathers, in: High Pressure Science and Technology, (ed. K. D. Timmerhous and M. S. Barbers), Plenum Press, New York, Vol. 2, 1979, p. 847.
[36]G. Franz *et al.*, in: Proceedings of the Fourth International Conference on Liquid and Amorphous Metals, Grenoble, 1980.
[37]V. E. Fortov, Modeli uravneniĭ sostoyaniya veshchestva (Model Equations of State for Matter), IkhF Akad. Nauk SSSR, Chernogolovka, 1979.
[38]V. A. Alekseev, V. G. Ovcharenko, and Yu. F. Ryzhkov, J. Phys. (Paris) **41**, 8, Suppl. C8-89 (1980).
[39]A. A. Likal'ter, Zh. Eksp. Teor. Fiz. **56**, 240 (1969) [Sov. Phys. JETP **29**, 133 (1969)].
[40]Yu. G. Krasnikov, Zh. Eksp. Teor. Fiz. **73**, 516 (1977) [Sov. Phys. JETP **46**, 270 (1977)].
[41]V. K. Gryaznov, Zh. Eksp. Teor. Fiz. **78**, 573 (1980) [Sov. Phys. JETP **51**, 288 (1980)].
[42]V. K. Gryaznov and I. L. Iosilevskiĭ, Chisl. metody mekh. sploshn. sredy **4**, 166 (1973).
[43]V. E. Bespalov, V. K. Gryaznov, A. N. Dremin, and V. E. Fortov, Zh. Eksp. Teor. Fiz. **69**, 2059 (1975) [Sov. Phys. JETP **42**, 1046 (1975)].
[44]J. P. Hansen, in: Strongly Coupled Plasmas (ed. G. Kalman), Plenum Press, New York, 1978, p. 119.
[45]H. E. De Witt, in: Strongly Coupled Plasmas (ed. G. Kalman), Plenum Press, New York, 1978, p. 83.
[46]V. E. Fortov *et al.*, Zh. Eksp. Teor. Fiz. **71**, 225 (1976) [Sov. Phys. JETP **44**, 116 (1976)].
[47]V. B. Mintsev and V. E. Fortov, Pis'ma Zh. Eksp. Teor. Fiz. **30**, 401 (1979) [JETP Lett. **30**, 375 (1979)].
[48]N. F. Carnahan and K. E. Starling, J. Chem. Phys. **51**, 632 (1969).
[49]V. E. Fortov, A. N. Dremin, A. A. Leont'ev, and S. V. Pershin, Pis'ma Zh. Eksp. Teor. Fiz. **20**, 30 (1974) [JETP Lett. **20**, 13 (1974)].
[50]B. A. Glushak, M. V. Zhernokletov, and V. N. Zubarev, in:

Doklady I Vsesoyuznogo simpoziuma po impul'snym davleniyam (Proceedings of the First All-Union Symposium on Pulsed Pressures), Nauka, Moscow, 1974, p. 87.
[51]A. V. Bushman, V. E. Fortov, and A. L. Ni, in: Eighth International Colloquium on Gas Dynamics of Explosions and Reactive Systems: Abstracts, Minsk, 1981, p. 156.
[52]B. V. Zelener, Teplofiz. Vys. Temp. 15, 893 (1977).
[53]N. V. Ermokhin *et al.*, Teplofiz. Vys. Temp. 9, 665 (1971).
[54]V. A. Alekseev *et al.*, High Temp. High Pressure 7, 676 (1975).
[55]H. Renkert, F. Hensel, and E. U. Frank, Ber. Bunsenge. Phys. Chem. 75, 507 (1971).
[56]V. A. Sechenov, É. E. Son, and O. E. Shchekotov, Pis'ma Zh. Tekh. Fiz. 1, 891 (1975) [Sov. Tech. Phys. Lett. 1, 388 (1975)].
[57]A. N. Lagar'kov and I. T. Yakubov, in: Khimiya plazmy (Plasma Chemistry) (ed. B. M. Smirnov), Atomizdat, Moscow, Vol. 7, 1980, p. 75.
[58]V. A. Alekseev and A. A. Vedenov, Usp. Fiz. Nauk **102**, 665 (1970) [*sic*].
[59]B. M. Smirnov, Dokl. Akad. Nauk SSSR **195**, 75 (1970) [Sov. Phys. Dokl. 15, 1050 (1971)].
[60]A. G. Khrapak, Teplofiz. Vys. Temp. **17**, 1147 (1979).
[61]P. P. Kulik, G. É. Norman, and L. S. Polak, Khim. vys. energii **10**, 203 (1975).
[62]N. V. Iermohin, B. M. Kovalev, and P. P. Kulik, in: Twelfth International Conference on Phenomena in Ionized Gases, Contributed Papers, Eindhoven, New York, American Elsevier, 1975, p. 184.
[63]V. K. Gryaznov, G. L. Gutsev, and V. E. Fortov, Teplofiz. Vys. Temp. **18**, 733 (1980).
[64]I. T. Yakubov, in: Khimiya plazmy (Plasma Chemistry) (ed. B. M. Smirnov), Atomizdat, Moscow, Vol. 1, 1974, p. 120.
[65]A. G. Khrapak and I. T. Yakubov, Teplofiz. Vys. Temp. **9**, 1139 (1971).
[66]F. Hensel and E. U. Franck, Rev. Mod. Phys. **40**, 697 (1968).
[67]I. K. Kikoin and A. P. Senchenkov, Fiz. Met. Metalloved. **24**, 843 (1967).
[68]H. Uchtmann and F. Hensel, Phys. Lett. **A53**, 239 (1975).
[69]A. N. Lagar'kov and A. K. Sarychev, Teplofiz. Vys. Temp. **16**, 953 (1978).
[70]A. A. Likal'ter, Teplofiz. Vys. Temp. **16**, 1169 (1978); **19**, 746 (1981).
[71]I. T. Yakubov, Dokl. Akad. Nauk SSSR **247**, 841 (1979) [Sov. Phys. Dokl. **24**, 634 (1979)].
[72]A. N. Lagar'kov and A. K. Sarychev, Zh. Eksp. Teor. Fiz. **68**, 641 (1975) [Sov. Phys. JETP **41**, 317 (1975)].
[73]A. N. Lagar'kov and A. K. Sarychev, Teplofiz. Vys. Temp. **16**, 903 (1978).
[74]V. A. Alekseev *et al.*, Pis'ma Zh. Eksp. Teor. Fiz. **12**, 351 (1970) [*sic*].
[75]L. I. Bolshov and A. N. Starostin, in: Tenth International Conference on Ionization Phenomena in Gases, Contributed Papers, Paper N 4.2.2.4, Oxford, 1971.
[76]A. Herrmann *et al.*, J. Chem. Phys. **68**, 2327 (1978).
[77]A. N. Lagar'kov and A. K. Sarychev, Teplofiz. Vys. Temp. **17**, 429 (1979).
[78]F. E. Neal and N. E. Cusack, J. Phys. F **9**, 85 (1979).
[79]H. P. Pfeifer, W. F. Freyland, and F. Hensel, Phys. Lett. **A43**, 111 (1973).
[80]A. L. Khomkin, Teplofiz. Vys. Temp. **12**, 870 (1974).
[81]J. B. Bernstein, Phys. Fluids **12**, 64 (1969).
[82]H. A. Gould and H. E. Dewitt, Phys. Rev. **155**, 68 (1967); R. H. Williams and H. E. Dewitt, Phys. Fluids **12**, 2326 (1969).
[83]F. J. Rogers, H. E. Dewitt, and D. B. Boercker, Phys. Lett. **A82**, 31 (1981).
[84]Yu. L. Klimontovich, Kineticheskaya teoriya neideal'nykh gazov i plazmy (Kinetic Theory of Nonideal Gases and Plasmas), Nauka, Moscow, 1975.
[85]G. Ropke, W. Ebeling, and W. D. Kraeft, Physica (Utrecht) **A101**, 243 (1980).
[86]A. L. Khomkin, Teplofiz. Vys. Temp. **16**, 37 (1978).
[87]A. S. Kaklyugin and G. É. Norman, Teplofiz. Vys. Temp. **11**, 238 (1973).
[88]V. S. Vorob'ev and A. L. Khomkin, Fiz. Plazmy 3, 885 (1977) [Sov. J. Plasma Phys. 3, 499 (1977)].
[89]A. A. Bakeev and R. E. Rovinskiĭ, Teplofiz. Vys. Temp. 8, 1121 (1979).
[90]M. M. Popovic, S. S. Popovic, and S. M. Vucovic, Fizika (Zagreb) **6**, 29 (1974).
[91]R. Radtke and K. Günter, Beitr. Plasmaphys. 15, 299 (1975).
[92]B. E. Tkachenko *et al.*, Fiz. goreniya i vzryva No. 5, 763 (1976).
[93]Yu. V. Ivanov *et al.*, Zh. Eksp. Teor. Fiz. **71**, 216 (1976) [Sov. Phys. JETP **44**, 112 (1976)].
[94]V. A. Alekseev *et al.*, J. Phys. (Paris) **40**, 8, Suppl. C8-91 (1978).
[95]V. B. Mintsev, V. E. Fortov, and V. K. Gryaznov, Zh. Eksp. Teor. Fiz. **79**, 116 (1980) [Sov. Phys. JETP 52, 59 (1980)].
[96]N. V. Ermokhin *et al.*, Teplofiz. Vys. Temp. **15**, 695 (1977).
[97]R. V. Mitin *et al.*, Teplofiz. Vys. Temp. **13**, 706 (1975).
[98]P. P. Ogurtsova *et al.*, Teplofiz. Vys. Temp. **12**, 680 (1974).
[99]S. I. Andreev and T. V. Gavrilova, Teplofiz. Vys. Temp. **13**, 176 (1975).
[100]V. K. Gryaznov, Yu. V. Ivanov, A. N. Starostin, and V. E. Fortov, Teplofiz. Vys. Temp. **14**, 643 (1976).
[101]M. Baus, J. P. Hansen, and L. Siogren, Phys. Lett. **A82**, 180 (1981).
[102]V. S. Rogov, Teplofiz. Vys. Temp. **8**, 689 (1970).
[103]Yu. L. Klimontovich and W. Ebeling, Zh. Eksp. Teor. Fiz. **63**, 905 (1972) [Sov. Phys. JETP **36**, 476 (1973)]; Yu. L. Klimontovich and D. Kremp, Physica **A41**, 412 (1982).
[104]S. A. Maev, Zh. Tekh. Fiz. **40**, 567 (1970) [Sov. Phys. Tech. Phys. **15**, 438 (1970)].
[105]L. M. Biberman and G. É. Norman, Usp. Fiz. Nauk **91**, 193 (1967) [Sov. Phys. Usp. **10**, 52 (1967)].
[106]F. Hensel, Ber. Bunsenge. Phys. Chem. **76**, 847 (1971).
[107]F. Hensel, Phys. Lett. **A31**, 88 (1970).
[108]H. Ikezi *et al.*, Phys. Rev. **A18**, 2494 (1978).
[109]F. Hensel, in: Proceedings of the Eighth Symposium on Thermo-physical Properties, Gaithersburg, June, 1981.
[110]J. Popielawski, H. Uchtmann, and F. Hensel, Ber. Bunsenges. Phys. Chem. **83**, 123 (1979).
[111]R. N. Bhatt and T. M. Rice, Phys. Rev. **B20**, 466 (1979).
[112]H. Uchtmann and F. Hensel, Phys. Mag. **B42**, 583 (1980).
[113]S. I. Andreev, T. V. Gavrilova, and V. E. Gavrilov, in: Tezisy dokladov IV Vsesoyuznoĭ konferentsii po fizike nizkotemperaturnoĭ plazmy (Abstracts of Papers Presented at the Fourth All-Union Conference on the Physics of Low-Temperature Plasmas), Vol. 1, Kiev, 1975, p. 16.
[114]S. I. Andreev, Zh. Tekh. Fiz. **45**, 1010 (1975) [Sov. Phys. Tech. Phys. 20, 636 (1975)].
[115]V. M. Batenin and V. P. Minaev, Teplofiz. Vys. Temp. **15**, 647 (1977).
[116]V. E. Bespalov, V. K. Gryaznov, and V. E. Fortov, Zh. Eksp. Teor. Fiz. **76**, 140 (1979) [Sov. Phys. JETP **49**, 71 (1979)].
[117]G. A. Kobzev, Yu. K. Kurilenkov, and G. É. Norman, Teplofiz. Vys. Temp. **15**, 193 (1977).
[118]D. Schluter, Z. Phys. **210**, 80 (1968).
[119]G. A. Kobzev and Yu. K. Kurilenkov, Teplofiz. Vys. Temp. **16**, 458 (1978).
[120]Yu. K. Kurilenkov and V. P. Minaev, Zh. Eksp. Teor. Fiz. **74**, 563 (1978) [Sov. Phys. JETP **47**, 295 (1978)].
[121]V. S. Lisitsa, Usp. Fiz. Nauk **122**, 449 (1977) [Sov. Phys. Usp. 20, 603 (1977)].
[122]B. W. Shore, J. Phys. B **8**, 2023 (1975).
[123]G. Bekefi, Radiation Processes in Plasmas, Wiley, New York, 1966 (Russ. Transl. Mir, Moscow, 1971).
[124]F. E. Höne and R. Zimmerman, Teplofiz. Vys. Temp. **20**, *sic* (1982).

[125]B. K. Tkachenko *et al.*, in: Tezisy dokladov VI Vsesoyuznoĭ konferentsii po dinamike izluchayushchego gaza (Abstracts of Papers Presented at the Sixth All-Union Conference on the Dynamics of Radiating Gases), Moscow, 1980.
[126]R. Radtke and K. Günter, in: Fifteenth International Conference on Phenomena in Ionized Gases, Contributed papers, Vol. 1, Minsk, 1981, p. 353.
[127]V. E. Gavrilov and T. V. Gavrilova, in: Fifteenth International Conference on Phenomena in Ionized Gases, Contributed papers, Vol. 1, Minsk, 1981, p. 339.
[128]V. A. Sechenov, in: Fifteenth International Conference on Phenomena in Ionized Gases, Contributed papers, Vol. 1, Minsk, 1981, p. 357.
[129]H. R. Griem, Plasma Spectroscopy, Academic, New York, 1964 (Russ. Transl. Atomizdat, Moscow, 1969).
[130]I. T. Iakubov, Beitr. Plasmaphys. **17**, 221 (1977).
[131]I. M. Rutkevich and O. A. Sinkevich, Teplofiz. Vys. Temp. **18**, 27 (1980).
[132]V. M. Atrazhev and I. T. Yakubov, Teplofiz. Vys. Temp. **18**, 16 (1980).
[133]S. G. Barol'skiĭ *et al.*, Teplofiz. Vys. Temp. **14**, 702 (1976).
[134]G. A. Kobzev and Yu. K. Kurilenkov, Teplofiz. Vys. Temp. **16**, 458 (1978).
[135]K. I. Shchelkin, in: Mekhanika v SSSR za 50 let. (Mechanics Over Fifty Years in the USSR), Nauka, Moscow, 1967, p. 343.
[136]G. A. Pavlov, V. E. Fortov, and A. A. Ovchinnikov, Dokl. Akad. Nauk SSSR **251**, 1085 (1980) [Sov. Phys. Dokl. **25**, 241 (1980)].
[137]S. A. Bostandzhiyan, A. G. Merzhanov, and S. N. Khudyaev, Dokl. Akad. Nauk SSSR **163**, 133 (1965).
[138]G. A. Pavlov and A. A. Ovchinnikov, Teplofiz. Vys. Temp. 1981.
[139]V. E. Fortov, Teplofiz. Vys. Temp. **10**, 168 (1972).
[140]Y. Horie, J. Phys. Chem. Solids **28**, 1569 (1967).
[141]V. N. Zharkov and V. A. Kalinin, Uravneniya sostoyaniya tverdykh tel pri vysokikh davleniyakh i temperaturakh (Equations of State of Solids at High Pressures and Temperatures), Nauka, Moscow, 1968.
[142]Ya. B. Zel'dovich and Yu. P. Raĭzer, Fizika udarnykh voln i vysokotemperaturnykh gidrodinamicheskikh yavleniĭ (Physics of Shock Waves and High-Temperature Hydrodynamic Phenomena), Nauka, Moscow, 1967.
[143]G. Ya. Galin, Dokl. Akad. Nauk SSSR **119**, 1106 (1958) [Sov. Phys. Dokl. **3**, 244 (1958)]; **120**, 730 (1958) [Sov. Phys. Dokl. **3**, 503 (1959)].
[144]A. D. Sidorenko, Dokl. Akad. Nauk SSSR **178**, 818 (1968) [Sov. Phys. Dokl. **13**, 117 (1968)].
[145]A. G. Ivanov and S. A. Novikov, Zh. Eksp. Teor. Fiz. **40**, 1880 (1961) [Sov. Phys. JETP **13**, 1321 (1961)].
[146]S. S. Kutateladze, A. A. Borisov, and V. E. Nakoryakov, Dokl. Akad. Nauk SSSR **252**, 595 (1980) [Sov. Phys. Dokl. **25**, 392 (1980)].
[147]S. P. D'yakov, Zh. Eksp. Teor. Fiz. **27**, 288 (1959) [*sic*].
[148]S. V. Iordanskiĭ, Prikl. Mat. Mekh. **21**, 465 (1957).
[149]V. M. Kantorovich, Zh. Eksp. Teor. Fiz. **33**, 1525 (1957) [Sov. Phys. JETP **6**, 1179 (1958)].
[150]J. J. Erpenbeck, Phys. Fluids **5**, 1181 (1962); **6**, 1368 (1963).
[151]G. W. Swan and G. R. Fowles, Phys. Fluids **18**, 28 (1975).
[152]E. I. Zababakhin and V. A. Simonenko, Zh. Eksp. Teor. Fiz. **52**, 1317 (1967) [Sov. Phys. JETP **25**, 876 (1967)].
[153]G. R. Fowles, Phys. Fluids **19**, 227 (1976).
[154]V. E. Fortov, A. L. Ni, and S. G. Sugak, Cited in Ref. 51, p. 163.
[155]T. N. Fortova, A. N. Dremin, and V. E. Fortov, Chisl. metody mekh. sploshnoĭ sredy **4**, 143 (1973).
[156]S. V. Bobrovskiĭ and V. M. Goglev, Fiz. goreniya i vzryva **3**, 594 (1967).
[157]D. A. Kirzhnits, Usp. Fiz. Nauk **104**, 489 (1971) [Sov. Phys. Usp. **14**, 512 (1971)].
[158]V. E. Fortov, Zh. Tekh. Fiz. **11**, 333 (1972) [*sic*].
[159]B. N. Lomakin, V. E. Fortov, and O. E. Shchekotov, Teplofiz. Vys. Temp. **9**, 628 (1980).
[160]R. W. Griffiths, R. J. Sandeman, and H. G. Hornung, J. Phys. D **9**, 1681 (1976).
[161]G. K. Tumakaev, Pis'ma Zh. Tekh. Fiz. **6**, 1239 (1980) [Sov. Tech. Phys. Lett. **6**, 531 (1980)].
[162]L. Spitzer Jr., Physics of Fully Ionized Gases, Interscience, New York, 1962 (Russ. Transl. Mir, Moscow, 1963).

Translated by Dave Parsons